REVIEW

Check for updates

Self-assembled monolayers as hole-transporting materials for inverted perovskite solar cells

Zhong-Rui Lan,[ab] Jiang-Yang Shao [iD] *[a] and Yu-Wu Zhong [iD] *[ab]

The emerging perovskite solar cells (PSCs) have been explored as the most promising photovoltaic technology in the past decade, with the sharp increase of the power conversion efficiency (PCE) from 3.8% to certified 26.1%, comparable to that of crystalline silicon solar cells. Compared to conventional PSCs, inverted PSCs show attractive advantages, such as high device stability, negligible hysteresis and excellent compatibility with flexible and tandem devices. Self-assembled monolayers (SAMs) have been considered as one of the most promising hole-transporting materials (HTMs) for inverted PSCs owing to their low costs and material consumption and simple device fabrication with high PCEs. This review summarizes the recent developments in highly efficient SAMs as HTMs for inverted PSCs. On the basis of the anchoring group, three categories of SAMs are identified and discussed: SAMs with phosphonic acid, SAMs with carboxylic acid, and SAMs based on other anchoring groups. Finally, a future outlook of SAMs for high-performance inverted PSCs is provided. We hope that this review will be useful for the further design of SAMs toward the eventual commercialization of PSCs.

Design, System, Application

Hole-transporting materials (HTMs) are an essential component in perovskite solar cells (PSCs) where they play a decisive role in device stability, defect passivation, perovskite crystallization and hole extraction and transportation. The development of efficient, stable and low-cost HTMs is of vital importance for propelling PSCs toward commercialization. Compared to conventional HTMs, SAM HTMs exhibit attractive advantages such as low cost, simple fabrication and low material consumption. Moreover, SAM HTMs exhibit plenty of impressive results in improving the device performance in both single-junction and tandem PSCs. Here, recent progress of SAMs as HTMs in PSCs is summarized. The brief discussion of the design principles and development of SAMs is presented by different anchoring groups and molecular skeletons. Finally, a future outlook toward highly efficient SAMs in PSCs is proposed. The objective of this review is to provide guidance to readers on exploring new avenues for the discovery of novel SAMs, to aid in the future development and advancement of PSCs for commercial applications.

1 Introduction

The energy demand is increasing rapidly with the development of technology and economy. Photovoltaics (PVs) are considered to be the most abundant climate-neutral energy since fossil fuels are resource-limited and cause serious environmental problems.[1,2] Great efforts have been undertaken to improve the power conversion efficiency (PCE), stability and scalability of solar cells.[3,4] Among them, the emerging perovskite solar cells (PSCs) have been explored as the most promising PV technology in the past decade, with the sharp increase of the PCE from 3.8% to certified 26.1%, comparable to that of crystalline silicon solar cells.[5-7]

Generally, a typical PSC device consists of electrodes, a hole-transporting layer (HTL), a light-absorbing perovskite layer and an electron-transporting layer (ETL).[8,9] According to the deposition sequence of HTL and ETL, PSCs are commonly

[a] Beijing National Laboratory for Molecular Sciences, CAS Research/Education Center for Excellence in Molecular Sciences, Institute of Chemistry, Chinese Academy of Sciences, 2 Bei Yi Jie, Zhong Guan Cun, Haidian District, Beijing 100190, China. E-mail: shaojiangyang@iccas.ac.cn, zhongyuwu@iccas.ac.cn
[b] School of Chemical Sciences, University of Chinese Academy of Sciences, No.19(A) Yuquan Road, Shijingshan District, Beijing 100049, China

Zhong-Rui Lan obtained his bachelor's degree from the University of Chinese Academy of Sciences in 2021. He is currently a doctor graduate student at the Institute of Chemistry, Chinese Academy of Sciences (ICCAS) under the supervision of Prof. Yu-Wu Zhong. His research interest focuses on material and device fabrication of efficient and stable perovskite solar cells.

Zhong-Rui Lan

divided into two architectures, conventional (n–i–p) structure and inverted (p–i–n) structure, in which n–i–p PSCs either have a mesoporous or planar structure referring to the type of ETL.[10–12] Compared to conventional PSCs, inverted devices show attractive advantages, such as high device stability, negligible hysteresis and excellent compatibility with flexible and tandem devices.[13–15] However, the PCEs of inverted PSCs still lag behind those of n–i–p devices, mainly due to the relatively lower open-circuit voltage (V_{oc}) and fill factor (FF) dominated by the charge recombination at the perovskite/charge-transporting layer interface.[16–20]

Very recently, the record PCE of inverted PSCs has exceeded the 25% barrier, thanks to the development of new hole-transporting materials (HTMs).[21–23] In general, the HTL extracts the holes and blocks the electrons from the electrode, requiring the suitable highest occupied molecular orbital (HOMO) and lowest unoccupied molecular orbital (LUMO) energy levels of the HTMs to match with those of the electrode and perovskite.[24–27] The HTL in n–i–p devices is exposed to oxygen and moisture, while in p–i–n devices, it acts as the base surface for the deposition of the perovskite layer. Therefore, suitable surface wettability of HTLs in inverted PSCs is necessary for the deposition and crystallization of the perovskite atop.[28–30] Moreover, the transmittance of the HTL should be as high as possible to increase the light absorption of the perovskite layer since sunlight needs to pass through the HTL first.[31]

The most common and effective HTMs used in p–i–n devices can be divided into two main categories: inorganic materials and organic molecules. Inorganic HTMs (such as NiO_x) usually possess high thermal stability and transparency. Nevertheless, most of the inorganic HTLs are fabricated by either a high-temperature or high-vacuum process.[32–36] Due to the relatively low intrinsic conductivity, poor wettability and high surface activity caused by the solution-process, only limited numbers of inorganic materials have been developed as efficient HTMs.[37] As for the widely used NiO_x, former studies have revealed that Ni^{3+} species on

the surface of NiO_x can react with organoiodide species in perovskite precursors, resulting in a defective NiO_x/perovskite interface.[38] On the contrary, organic HTMs can be fabricated with a solution-process at low temperature and modified by finely changing the molecular design, exhibiting great potential in performance, stability and scalability. Organic HTMs mainly include polymers, small molecules and self-assembled monolayers (SAMs). For a long period of time, polymer HTMs such as PEDOT:PSS (poly(3,4-ethylenedioxythiophene):poly(styrenesulfonate)) and PTAA (poly-[bis(4-phenyl)(2,4,6-trimethylphenyl)amine]) have been dominant in inverted PSCs.[39,40] With PTAA HTM, Pan *et al.* fabricated PSCs with a record PCE of 25.45% (certified 24.9%).[41] Nevertheless, the poor wettability of PTAA remains a problem. Special composition engineering of perovskites or surface treatment need to be carried out to improve the surface wettability to achieve high PCE.[42] In addition, the small-molecule HTL is often damaged by the polar solvents used in perovskite precursor solutions, and its device performance typically lags behind that with polymer HTMs. New kinds of HTMs for inverted PSCs, therefore, are required for further breakthrough. Recently emerged SAM-HTMs exhibit plenty of impressive results in improving the device performance in both single-junction and tandem PSCs.[43,44]

SAMs are ordered organic molecules with a thickness of one or few layers of molecules arrays formed by spontaneous adsorption onto the substrate surface from a vapor or liquid phase.[45] Unlike common small molecules or polymer HTMs, the molecules that are used to form SAMs are functionalized to link with the substrate *via* chemical bonding to afford the HTL. The stable and thin HTL can not only resist the damage caused by the perovskite precursor solutions but also provides a robust and smooth surface for the growth and crystallization of perovskite. Because of its extremely thin thickness, the HTL formed with SAMs can efficiently transfer the hole and reduce the charge accumulation at the perovskite/HTL interface, also decreasing the loss of incident light. Besides, SAMs exhibit attractive advantages such as

Jiang-Yang Shao received his Ph.D. Degree from ICCAS in 2014 with Prof. Yu-Wu Zhong. After that, he worked as an assistant professor in the same research group and was promoted as an associate professor in 2019. His current research interests focus on perovskite solar cells.

Jiang-Yang Shao

Yu-Wu Zhong obtained his Ph.D. degree in 2004 from Shanghai Institute of Organic Chemistry, Chinese Academy of Sciences. After working as a postdoctoral associate at the University of Tokyo (2004–2006) and Cornell University (2006–2009), respectively, he started his independent career in 2009 and works at present as a full professor at ICCAS. His research interests focus on the syntheses and applications of molecular materials in mixed-valence chemistry, near-infrared electrochromism, organic nanophotonics, and perovskite solar cells.

Yu-Wu Zhong

This journal is © The Royal Society of Chemistry and IChemE 2023

Mol. Syst. Des. Eng., 2023, **8**, 1440–1455 | **1441**

low cost, simple fabrication and low material consumption.

Herein, this review summarizes the recent developments in highly efficient SAM-HTMs. SAMs are classified based on the different anchoring groups, which differ from previous reviews based on different functional groups.[13] A brief discussion and summary of the design principles and development of SAM-HTMs are presented. At the end, a brief perspective on the future development of SAM-HTMs for highly efficient and stable p–i–n PSCs is provided.

2 Self-assembled monolayer HTMs

Generally, SAMs consist of three parts, namely (1) an anchoring group which connects the molecule to the substrate, (2) a linkage which connects the anchoring group and terminal group, (3) a functional group (or called terminal group) which modifies the surface and interface properties, directly in contact with the upper perovskite layer (Fig. 1). Currently, different types of anchoring groups are used in SAMs including thiol, carboxylic acid, phosphoric acid, silane and boric acid. The type of anchoring group will affect the interfacial dipole, recombination energy losses, contact resistance, coverage ratio and work function of the substrate.[46,47] The linkage commonly used for PSCs includes a nonconjugated aliphatic group or conjugated aromatic unit, which affects the geometry and packing of the molecules on the substrates. So far, the most commonly used functional groups are electron-rich aromatics, such as carbazole, triphenylamine, phenothiazine, *etc.*[13] The aromatic units can not only extract/transport holes, but also form new surfaces with perovskite as growth templates for subsequent perovskite layers. In addition, the functional groups can form a dipole moment to tune the energy level.

A SAM-based HTL can be prepared with a vapor or liquid-based deposition procedure. The former method requires the exposure of the clean substrate to an atmosphere saturated with SAM molecules, followed by post-annealing to strengthen the bonding to the substrate.[48,49] The liquid-phase method mainly includes dip-coating and spin-coating. Dip-coating is usually applied to mesoporous substrates, in which the substrate is immersed into the HTM solution, allowing the molecules to self-assemble on the surface of the substrate to form SAMs. Tuning the choice of solvent, the concentration of HTM molecules and the dipping time can easily modulate the process without any specialized equipment.[50] As for spin-coating, the HTM solution is dispensed to the substrate to produce a uniform film. In both
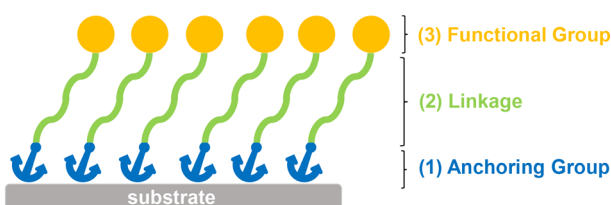
methods, the excessive unbonded molecules are removed by solvent after a thermal annealing process to strength the bonding. Thanks to its convenient and rapid deposition, spin-coating is often used in planar PSCs.[51]

2.1 SAM-HTMs based on phosphonic acid anchoring groups

Phosphonic acid is often used as the anchoring group to assist the formation of densely packed, uniform monolayers on various oxide surfaces by strong bidentate/tridentate immobilization.[52] The chemical adsorption binding modes of phosphonic acid and metal oxides were studied using various techniques, such as polarization-modulated infrared reflectance adsorption spectroscopy and X-ray photoelectron spectroscopy.[53] The applications of phosphonic acid in various applications have been well-established, including electrochromism and dye-sensitized solar cells.[54]

2.1.1 Carbazole. Although SAMs have been used in DSSCs and as ETL modifications in PSCs, the first SAM-HTM based PSC was reported in 2018. Getautis and co-workers designed and synthesized compound V1036 ((2-{3,6-bis[bis(4-methoxyphenyl)amino]-9H-carbazol-9-yl}ethyl)phosphonic acid) (Fig. 2a), using a carbazole unit as the building block, phosphonic acid as the anchoring group, ethyl as the linkage and dimethoxydiphenylamine unit as the functional group.[55] Carbazole is an ideal platform for SAM-HTMs due to its excellent hole-transporting capability, rigid skeleton and easy functionalization. V1036 exhibits good thermal stability with a high decomposition temperature (T_d = 343 °C). The formation of SAM was achieved by a dip-coating method. Compared to PTAA, V1036 shows a negligible influence on the absorption of ITO. Analysis of Fourier-transform infrared (FTIR) spectra of samples prepared in adsorption solutions containing different concentrations of V1036 have been performed. The vibrational bands of surface layers prepared
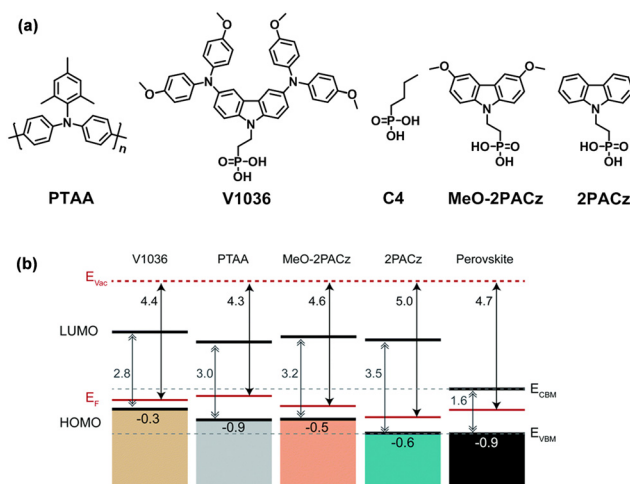
Fig. 1 Schematic representation of SAMs.

Fig. 2 (a) Chemical structures of PTAA, V1036, C4, MeO-2PACz and 2PACz. (b) Schematic representation of the band edge positions of the investigated SAMs. Reproduced with permission.[56] Copyright 2019 The Royal Society of Chemistry.

1442 | *Mol. Syst. Des. Eng.*, 2023, **8**, 1440–1455

This journal is © The Royal Society of Chemistry and IChemE 2023

from 0.1 and 1×10^{-3} M adsorption solutions are very similar both in peak positions and intensities. This suggests the absence of multilayer materials in the studied samples. A mixture of V1036 and butylphosphonic acid (C4) was used to optimize the ionization potential and wettability of the HTL. Finally, PSCs based on 10% V1036 and 90% C4 SAM achieved a PCE of 17.8% and a high FF of 81%.

Following this work, they further designed and synthesized two SAM-HTMs based on phosphonic acid and a carbazole unit (Fig. 2a), namely MeO-2PACz ([2-(3,6-dimethoxy-9*H*-carbazol-9-yl)ethyl]phosphonic acid) and 2PACz ([2-(9*H*-carbazol-9-yl)ethyl]phosphonic acid), outperforming PTAA.[56] In comparison to V1036, the smaller size of the functional group in MeO-2PACz and 2PACz enables better interface contact. These two SAMs not only provided a well-matched energy level but also reduced the non-radiative recombination at the interface (Fig. 2b). The SAM-HTL can be deposited by either spin-coating or dip-coating, combining reproducibility and ease of manufacture. A high V_{oc} of 1.19 V and PCE of 20.9% (certified 20.28%) were demonstrated by 2PACz-based triple-cation PSCs. Besides, an enhanced PCE of 21.1% was delivered by the MeO-2PACz-based inverted double-cation PSCs. By applying MeO-2PACz into a monolithic CIGSe/perovskite tandem solar cell, a certified stabilized PCE of 23.26% was achieved on an active area of 1.02 cm², demonstrating the ability of the SAM to achieve conformal deposition on the rough surface. Cross-sectional elemental maps deduced from the energy-dispersive X-ray spectroscopy (EDX) measurements of the fabricated devices can show whether the SAM covers the substrate conformally.[57] Especially in a peak-valley-shaped region of a tandem device, it is clear to see whether the corresponding elemental signal covers both the valley and peak conformally.

Albrecht *et al.* further investigated the influence of aliphatic chain length and different substitutions of the carbazole unit, and Me-4PACz ([4-(3,6-dimethyl-9*H*-carbazol-9-yl)butyl]phosphonic acid) was found to have the best performance among a series of carbazole-based molecules (Fig. 3a).[58] The accelerated hole-extraction paired with minimized nonradiative recombination at the HTL/perovskite interface effectively stabilizes the perovskite phase under long-term illumination and simultaneously enables high quasi-Fermi level splitting (Fig. 3b). Thus, the FF of p–i–n single-junction PSCs with the integration of Me-4PACz approaches up to 84%. At the same time, monolithic perovskite/silicon tandem solar cells with a high FF of 80% and a record certified PCE of 29.15% were realized. In addition to Pb-based PSCs, Loi *et al.* applied the Br-substituted carbazole SAM ([2-(3,6-dibromo-9*H*-carbazol-9-yl)ethyl]phosphonic acid, Br-2PACz) and 2PACz in mixed tin/lead (Sn/Pb) PSCs to replace the normally-used PEDOT:PSS.[59] By comparing two liquid-phase deposition methods, they found that the ITO surface was fully covered *via* liquid-phase immersion while the spin-coating process did not give a dense SAM-HTL, with only a portion of SAM molecules attaching to the substrate (Fig. 3c). The SAM-HTL thickness was estimated to be about 1 nm, which is equivalent to the molecular length
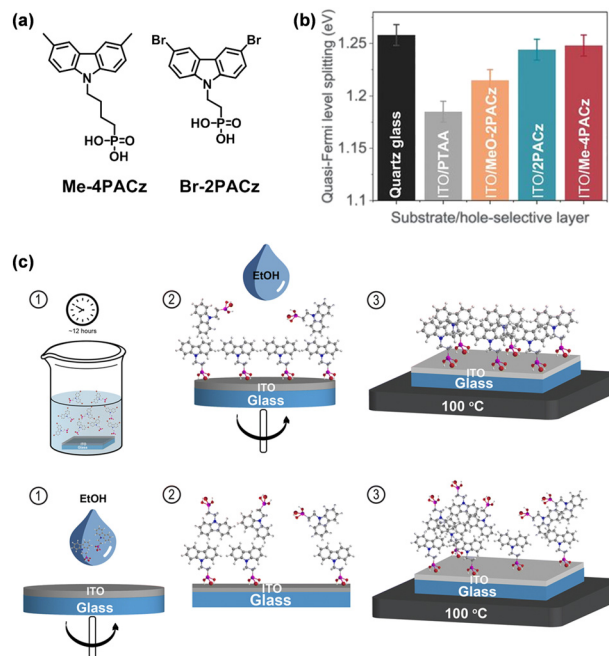

Fig. 3 (a) Chemical structures of Me-4PACz and Br-4PACz. (b) Quasi-Fermi level splitting values of perovskite films on a bare glass substrate and different hole-selective layers on the ITO electrode. Reproduced with permission.[58] Copyright 2020, The American Association for the Advancement of Science. (c) Schematic diagram of the deposition of 2PACz and Br-2PACz by liquid phase immersion (top) and spin coating (bottom). Reproduced with permission.[59] Copyright 2023 The Royal Society of Chemistry.

of Br-2PACz (11 Å). The perovskite layer deposited on such kind of dip-coating-processed dense HTL exhibits higher crystallinity, reduced pinhole density and larger grains. Sn/Pb PSCs based on dopant-free Br-2PACz HTL achieved a PCE of 19.51% with good storage stability maintaining 80% of its initial PCE in N₂ atmosphere for 176 days.

By engineering the position of the methoxy substituent in MeO-2PACz, Jen and co-workers reported HTM DC-PA ([[(2,7-dimethoxy-9*H*-carbazol-9-yl)methyl]phosphonic acid) with reduced electron-donating strength, leading to a favourable down-shifted HOMO level and an increased dipole moment.[60] An alky amine (6-(iodo-λ⁵-azanyl)hexanoic acid, IAHA) was used to aid the formation of a co-assembled monolayer to reduce the defects in the monolayer and simultaneously passivate the perovskite on top (Fig. 4a). With the introduction of IAHA, the HOMO energy level of co-SAM was decreased to −5.37 eV. In addition, a more homogeneous crystallization surface and larger crystals were observed for co-SAM-based perovskite films (Fig. 4b and c). PSCs based on DC-PA/IAHA achieved an excellent efficiency of 23.59%, while the DC-PA devices exhibited a champion PCE of 22.64%. To further increase the molecular dipole moment and strengthen the π–π interaction, Jen *et al.* developed two HTMs CbzPh ((4-(7*H*benzo[*c*]carbazol-7-yl)butyl)phosphonic acid) and CbzNaph ([4-(7*H*-dibenzo[*c*,*g*]carbazol-7-yl)butyl]phosphonic acid) by changing the carbazole unit of 4PACz with asymmetric or helical π-expansion (Fig. 4d).[61] The

This journal is © The Royal Society of Chemistry and IChemE 2023

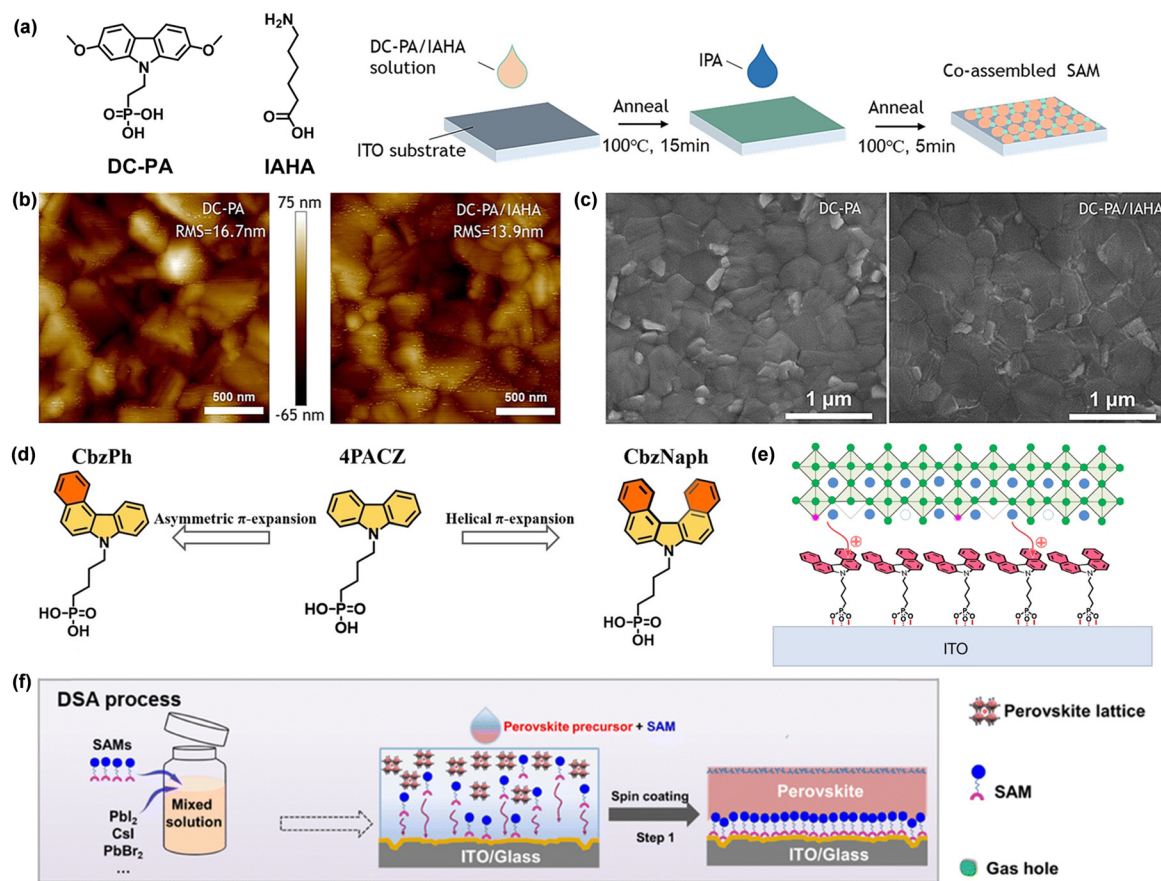*Mol. Syst. Des. Eng.,* 2023, **8**, 1440–1455 | **1443**

Fig. 4 (a) Molecular structures of DC-PA and IAHA (left) and schematic diagram for co-assemble monolayer fabrication (right). (b) AFM images and (c) SEM images of perovskite films deposited on DC-PA and DC-PA/IAHA substrates. Reproduced with permission.[60] Copyright 2022 Wiley-VCH GmbH. (d) Molecular structures of CbzPh and CbzNaph. Reproduced with permission.[61] Copyright 2022 Wiley-VCH GmbH. (e) Schematic of the interconnection between ITO, 4PADCB and perovskite. Reproduced with permission.[62] Copyright 2023 Springer Nature. (f) Schematic illustration of the dynamic self-assembly (DSA) strategy. Reproduced with permission.[63] Copyright 2023 The Royal Society of Chemistry.

helical π-expanded CbzNaph possessing a large molecular dipole (2.41 D), favorable HOMO energy level (−5.39 eV) for aligning with the perovskite layer and compact π–π stacking (π–π distance = 3.34 Å) tends to form a densely assembled layer. Therefore, PSCs employing CbzNaph exhibited an excellent champion PCE of 24.1% and improved stability.

Almost at the same time, Zhao *et al.* employed CbzNaph (they called it 4PADCB) as the HTL in the fabrication of all-perovskite tandem solar cells.[62] For all-perovskite tandem solar cells, the large V_{oc} losses and relatively low FF in wide-bandgap (WBG) PSCs limit the further improvement of PCE, especially in devices with large active areas (>1 cm^2). By introducing 4PADCB, the film coverage and surface wettability were both improved to enable fast hole extraction and suppress the interfacial nonradiative recombination at the HTL/perovskite interface (Fig. 4e). WBG PSCs based on 4PADCB showed a notable improvement both in V_{oc} (1.30 V) and FF (78.7%) on a centimeter-scale active area. Next, the optimized WBG PSCs were integrated into monolithic all-perovskite tandem solar cells (aperture area: 1.044 cm^2), and a champion efficiency of 27.0% was obtained (V_{oc} = 2.11 V, short-circuit current density (J_{sc}) = 5.37 mA cm^{-2} and FF =

83.13%). Moreover, the 4PADCB-based all-perovskite tandem solar cells maintained 80% of their initial efficiency after 415 h of continuous maximum power point (MPP) tracking, much longer than those of PTAA and 4PACz-based devices. In 2023, Tang and co-workers demonstrated a dynamic self-assembly strategy to simultaneously fabricate the SAM-HTL with BCB-C4PA (the same molecule named as CbzPh in Jen's work above) and perovskite layer (Fig. 4f).[63] This strategy not only improves the quality of perovskite films, but also passivates the defects at grain boundaries and/or interfaces. A champion PCE of 22.2% along with remarkable long-term environmental stability was achieved.

2.1.2 Phenothiazine. In addition to carbazole derivatives, phenothiazine or its derivatives are another kind of commonly used building block. A series of SAMs based on the phenothiazine moiety and different anchoring groups, namely TPT-S6, TPT-C6 and TPT-P6, were investigated by Zhu and co-workers (Fig. 5a).[64] TPT-P6 shows the fastest adsorption rate and highest loading amount to the ITO substrate among these molecules, correlated to the high adsorption energy of the phosphonic acid group on the ITO surface (Fig. 5b and c). With a triple-cation perovskite

1444 | *Mol. Syst. Des. Eng.*, 2023, **8**, 1440–1455

This journal is © The Royal Society of Chemistry and IChemE 2023

$Cs_{0.05}MA_{0.12}FA_{0.83}Pb(I_{0.85}Br_{0.15})_3$, they achieved a PCE of 21.43% (0.09 cm^2) with a V_{oc} of 1.125 V and FF of 81.08%. The PCE shows a small drop to 20.09% when enlarging the device area to 1.0 cm^2, demonstrating the large-area uniformity of the TPT-P6-based devices.

Considering the poor wettability of TPT-P6 caused by the large hydrophobic triphenylamine group and the long aliphatic chain, Hong et al. reported Br-2EPT ([2-(3,7-dibromo-10H-phenothiazin-10-yl)ethyl]phosphonic acid) by changing the functional group to bromo-substituted phenothiazine and shortening the hexyl chain to ethyl group (Fig. 6a).[65] Br-2EPT demonstrates a faster hole extraction, better energy alignment with perovskite and markedly passivated defects via halogen bonding and Pb–S interaction (Fig. 6b). The CsMAFA PSCs based on Br-2EPT (PCE = 22.44%) outperformed the device with PTAA (19.26%) and MeO-2PACz (21.16%) under similar fabrication conditions. Later they reported two HTMs containing O and Se, namely (2-(3,7-dibromo-10H-phenoxazine-10-yl)ethyl)phosphonic acid (Br-2EPO) and (2-(3,7-dibromo-10H-phenoselenazin-10-yl) ethyl)phosphonic acid (Br-2EPSe), to investigate the effect of heteroatoms on the molecular electronic structure and device performance (Fig. 6a).[66] It was found that the interaction energy between Br-2EPSe and the perovskite absorber is the strongest among the series. The perovskite layer on the Br-2EPSe SAM exhibits the lowest interfacial trap density and the longest charge carrier
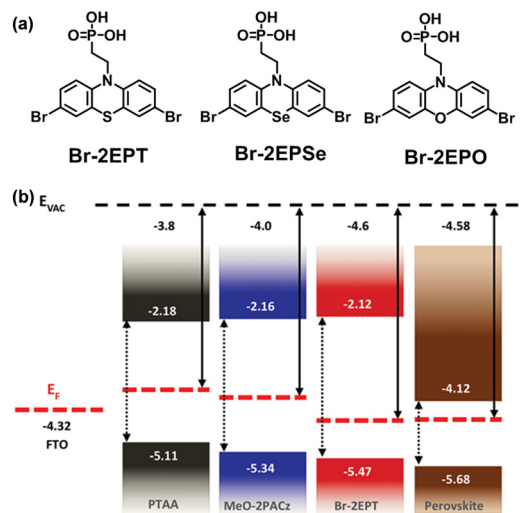

Fig. 6 (a) Molecular structures of Br-2EPT, Br-2EPSe, and Br-2EPO. (b) Energetic alignment of different SAMs and CsMAFA perovskite. Reproduced with permission.[65] Copyright 2022 Wiley-VCH GmbH.

lifetime. As a result, PSCs incorporating Br-2EPSe achieved a PCE of 22.73% (certified 22.26%) closely related to the enhanced V_{oc} and FF. Due to the superior interfacial properties of Br-2EPSe, the encapsulated devices retained about 96% of their initial efficiency after MPP tracking of 500 h under ambient conditions (15% to 25% relative humidity, RH).

2.1.3 Acridine and triazatruxene. Recently, He et al. synthesized a dimethylacridine-based HTM DMAcPA ([4-(2,7-dibromo-9,9-dimethylacridin-10(9H)-yl)butyl]phosphonic acid) with two Br substituents to construct all-round passivation of ground boundaries and well-matched perovskite/ITO contact (Fig. 7a).[67] Different from traditional SAM-HTMs, DMAcPA was used as a p-dopant to be added to the perovskite precursor solutions. During the chlorobenzene-quenched crystallization process, DMAcPA was extruded from the precursor solution to the grain boundaries and the bottom surface of the film (Fig. 7b). Due to the steric effect of the two methyl groups in DMAcPA, it prevents aggregation and jamming at grain boundaries in the film-formation process. The perovskite film doped with DMAcPA shows smoother morphology and diminished excess PbI$_2$ (Fig. 7c). DMAcPA doping can reduce deep-level hole trap density by suppressing defect states at grain boundaries and surfaces. The resulting PSCs based on DMAcPA attained a remarkable PCE of 25.86% (certified 25.39%). Generally, SAM molecules composed of functionalized π-conjugated cores tend to orient with their π-plane perpendicular (edge-on) to the metal oxide surface, probably resulting in inefficient orbital overlap with the perovskite surface and/or unsought hole-transporting in the lateral direction.[68,69] Wakamiya et al. designed a series of phosphonic acid functionalized star-shaped molecules with a triazatruxene core to investigate the effect of multiple anchoring groups on the molecular orientation.[70] 3PATAT-C3 with three
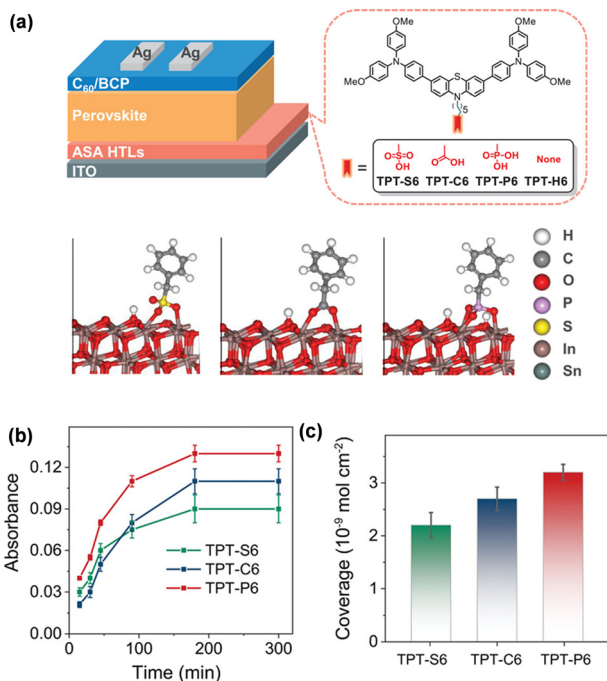

Fig. 5 (a) Schematic stack of the p–i–n structured PSCs with TPT-S6, TPT-C6, TPT-P6, and TPT-H6 (top) and theoretical adsorption mode of different anchor groups on the ITO (111) surface (bottom). (b) Maximum absorbance of HTMs after different deposition times. (c) The coverage of TPT-S6, TPT-C6, and TPT-P6 on ITO substrates. Reproduced with permission.[64] Copyright 2022 Wiley-VCH GmbH.

This journal is © The Royal Society of Chemistry and IChemE 2023

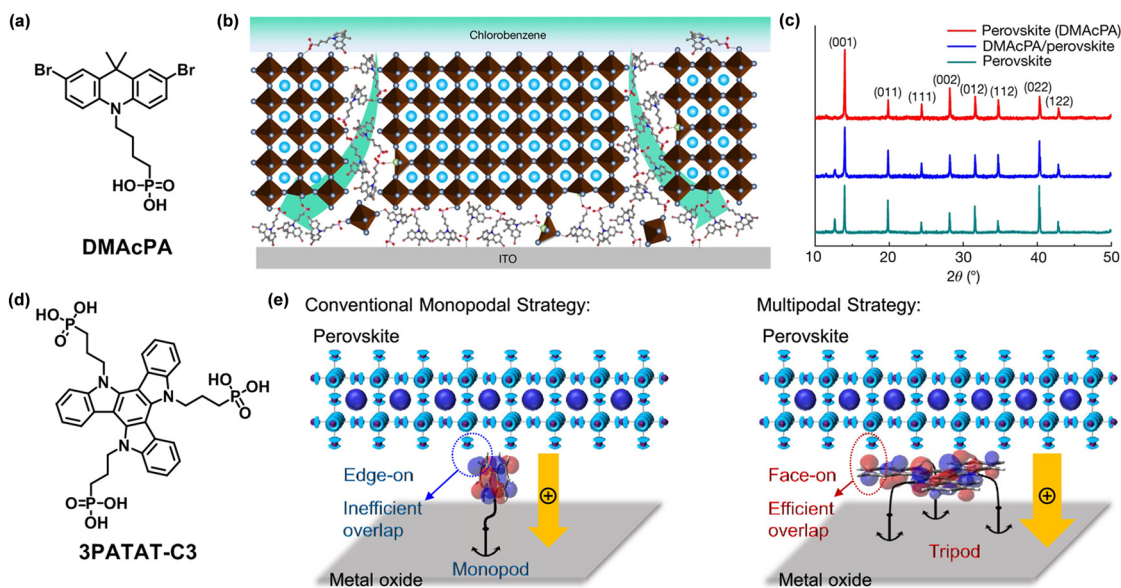Mol. Syst. Des. Eng., 2023, 8, 1440–1455 | 1445

Fig. 7 (a) Chemical structure of DMAcPA. (b) Schematic illustration of the molecule-extrusion model. (c) X-ray diffraction patterns of perovskite films deposited on ITO substrates. Reproduced with permission.[67] Copyright 2023 Springer Nature. (d) Chemical structure of 3PATAT-C3. (e) Molecular design concept for hole-collecting monolayer materials with the conventional monopodal strategy and multipodal strategy. Reproduced with permission.[70] Copyright 2023 American Chemical Society.

phosphonic acid groups was found to have a face-on alignment to the substrate, improving the hole extraction and reducing interface recombination (Fig. 7d and e). The inverted PSCs with 3PATAT-C3 realized a PCE of 23.0%.

Compared to the monopodal and dipodal PATAT derivatives, the devices using 3PATAT-C3 showed outstanding operational stability without any PCE loss after more than 2000 h of shelf-stability test.
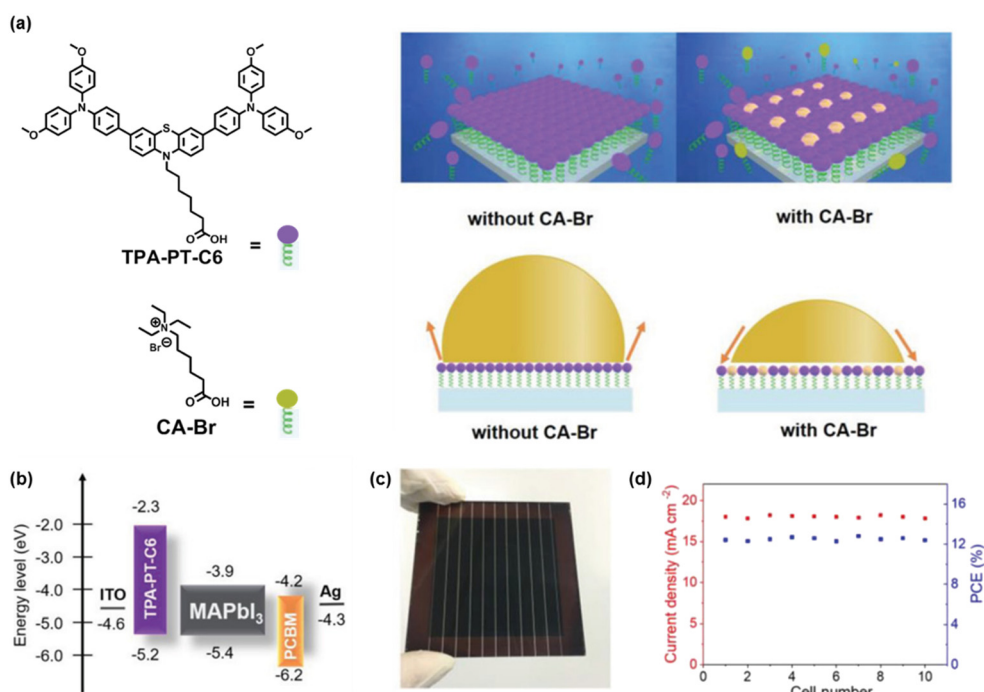

Fig. 8 (a) Molecular structures of TPA-PT-C6 and coadsorbent CA-Br (left), schematic illustration showing the deposition process of the self-assembled HTLs with and without a coadsorbent, and the increased wettability of the perovskite precursor on HTLs after coadsorption of CA-Br (right). (b) Energy diagram of different components in PSCs. (c) Photograph of a small module based on the co-assembled HTL. (d) The photocurrent density and efficiency of 10 subcells. Reproduced with permission.[71] Copyright 2020 Wiley-VCH GmbH.

1446 | *Mol. Syst. Des. Eng.*, 2023, **8**, 1440–1455

This journal is © The Royal Society of Chemistry and IChemE 2023

2.2 SAM-HTMs based on carboxylic acid anchoring groups

Besides the phosphonic acid unit, many SAMs are prepared using a carboxylic acid unit as the anchoring group. Zhu and co-workers designed a SAM-HTM, TPA-PT-C6 (7-(3,7-bis(4-(bis(4-methoxyphenyl)amino)phenyl)-10*H*-phenothiazin10-yl) heptanoic acid), by using carboxylic acid as the anchoring group, triphenylamine derived phenothiazine as the functional group and a hexyl group as the linkage.[71] TPA-PT-C6 co-assembles with hydrophilic ammonium salt CA-Br (6-carboxy-*N,N,N*-triethylhexan-1-aminium bromide) to form ultrathin uniform films with suitable wettability, facilitating large-area perovskite films with 100% coverage (Fig. 8a). The HOMO and LUMO energy levels of TPA-PT-C6 were estimated to be −5.20 and −2.34 eV, respectively (Fig. 8b). However, the coadsorbent CA-Br had no effect on its optical and electrochemical properties. The incorporation of CA-Br improves the mechanical and electronic contact at the HTL/ perovskite interface *via* the passivation of cation vacancies. Based on the co-assembled HTL, PSCs with active areas of 1.02 cm² achieved a PCE of 17.49% and showed good stability. The unencapsulated device maintained 89% of its initial efficiency after 120 days of storage under ambient conditions (30% RH). The scalability of the TPA-PT-C6/CA-Br co-assembled HTL was also evaluated by fabricating small modules with aperture areas of 36 cm², realizing a PCE of 12.67% (Fig. 8c). The almost identical results of the 10 subcells suggest that the uniformity of each layer in the module is quite good, indicating the superiority of TPA-PT-C6 for PSC scaling-up (Fig. 8d).

2,2′,7,7′-Tetrakis(*N,N′*-di-*p*-methoxyphenylamine)-9,9′-spirobifluorene (Spiro-OMeTAD) was widely used as the benchmark HTM in conventional PSCs for a long time. Due to its intrinsic low conductivity and hole mobility, Spiro-OMeTAD must be used in the presence of chemical dopants to increase the hole mobility, which usually compromises the long-term stability of the solar cells. Palomares *et al.* synthesized a Spiro-OMeTAD derivative as the SAM-HTM, namely Spiro-Acid, with a carboxylic acid unit as an anchoring group (Fig. 9a).[72] PSCs based on dip-coated Spiro-Acid achieved a PCE of 18.15% and an FF of 82.6% without bulk or interfacial passivation. The devices exhibited better stability under illumination due to the removal of PbI₂ from the perovskite.

Palomares *et al.* synthesized two SAM-HTMs, TPA (4,4″-bis(diphenyl amino)-1,1′:3′,1″-terphenyl-5′-carboxylic acid) and MC-43 (4′-[bis(2′,4′-dimethoxybiphenyl-4-yl)amino]-biphenyl-4-carboxylic acid), with carboxylic acid as the anchoring group, phenyl as the linkage and triphenylamine as the functional group (Fig. 9a).[46] The HOMO energy levels of TPA and MC-43 were determined as −5.33 and −5.11 eV, respectively (Fig. 9b). The optimized device with MC-43 exhibited a PCE of 17.3% with an FF of 80%, a V_{oc} of 1.07 V and a J_{sc} of 20.3 mA cm⁻², which was higher than the PCE of the corresponding device with TPA (15.9%). The authors attributed the high performance of MC-43 based devices to the better charge transfer capability of the HTL. Later in 2021, they replaced the triphenylamine unit of MC-43 with 1,3-dimethoxybenzene-substituted carbazole to develop EADR03 and EADR04 (Fig. 9a).[73] The carbazole and methoxy units act as electron donors, enabling a better charge-transporting ability and passivation effect than PTAA. In addition, the dimethoxybenzene moiety provides a miscible interface, allowing the formation of a homogenous and compact perovskite film. With the insertion of LiF and anti-reflection coating, the devices based on these two SAMs
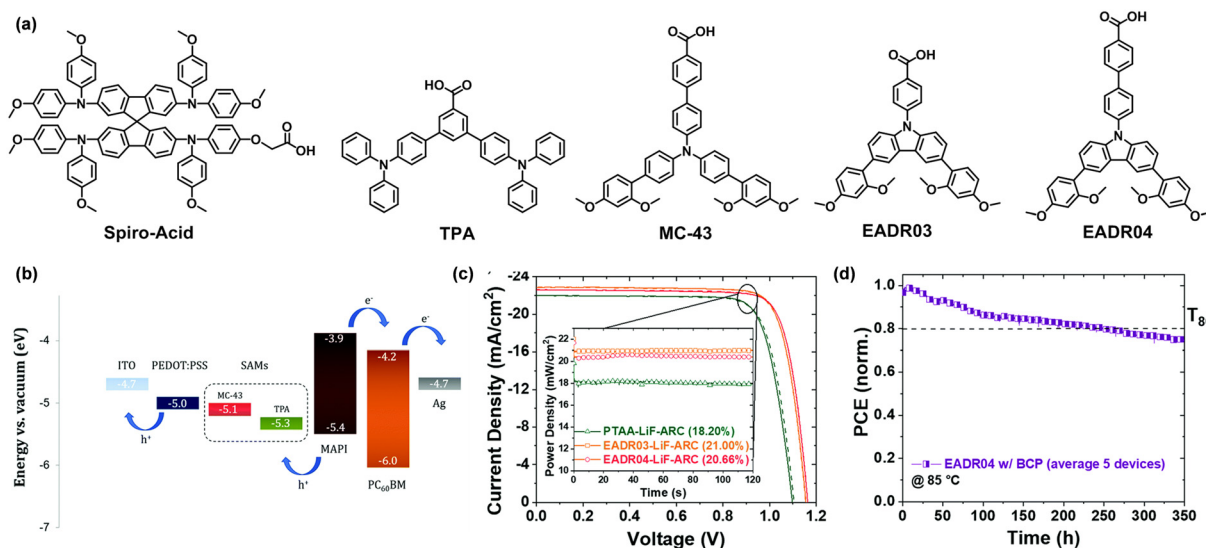

Fig. 9 (a) Chemical structures of Spiro-Acid, TPA, MC-43, EADR03, and EADR04. (b) Energy levels of different components in PSCs. Reproduced with permission.[46] Copyright 2019 The Royal Society of Chemistry. (c) Best *J–V* curves from PTAA, EADR03 and EADR04 with LiF and anti-reflection coating in the devices with quasi-steady state efficiency. (d) Long-term continuous MPP tracking of EADR04 with BCP at 85 °C. Reproduced with permission.[73] Copyright 2021 The Royal Society of Chemistry.

This journal is © The Royal Society of Chemistry and IChemE 2023

Mol. Syst. Des. Eng., 2023, **8**, 1440–1455 | **1447**

achieved PCE over 21% with a perovskite layer with a bandgap of 1.63 eV (Fig. 9c). Moreover, the device stability was determined superior to the PTAA-based reference devices. The EADR04-based devices retained 80% of their initial PCE after 250 h of MPP tracking at 85 °C (Fig. 9d).

Due to extensive π-conjugated macrocycles, excellent charge-transporting properties, and good thermal stability of porphyrin derivatives, a series of carboxylic acid-functionalized porphyrin SAM-HTMs (AC-1, AC-3, AC-5) were developed by Chou and co-workers (Fig. 10a).[74] It was found that the double-anchored porphyrins can passivate the perovskite layer and facilitate hole transfer (Fig. 10b). Among the three molecules, AC-5 with double anchoring groups and shorter alkyl chains efficiently strengthens the interaction with both ITO and perovskites, exhibiting the best performance. Small-area (0.1 cm^2) PSCs based on AC-5 achieved a champion PCE of 23.19% and an impressive FF of 84.05%. AC-5 was also applied to fabricate large-area devices (1.96 cm^2) to explore the scalability, achieving a PCE of 21.11%. The device also demonstrated outstanding stability after 600 h of continuous MPP tracking.

Zhao *et al.* designed a D–A-type molecule MPA2FPh-BT-BA (4-(7-(4-(bis(4-methoxyphenyl)amino)-2,5-difluorophenyl)benzo-[*c*][1,2,5]thiadiazol-4-yl)benzoic acid) as a SAM-HTM suitable to both WBG and narrow-bandgap (NBG) subcells for all-perovskite tandem solar cells (Fig. 11a).[75] MPA2FPh-BT-BA enables efficient hole extraction and passivation of interfacial defects in the WBG cells. Employed in NBG cells, it slows down the crystal growth and suppresses the oxidation of Sn^{2+} due to strong and targeted interaction with Sn^{2+} ions, leading to enhanced Sn–Pb perovskite quality and reduced interfacial losses (Fig. 11b). As a result, the monolithic all-perovskite tandem solar cells based on MPA2FPh-BT-BA delivered a high efficiency of 27.22% (certified 26.3%) and improved operational stability. Encapsulated tandem devices maintain 80% of their initial PCE after 301 h in air atmosphere, exhibiting much
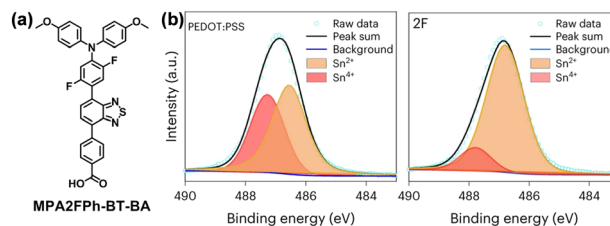

Fig. 11 (a) Molecular structure of MPA2FPh-BT-BA. (b) Sn 3d5/2 XPS spectra of different NBG perovskite films deposited on PEDOT:PSS and MPA2FPh-BT-BA. Reproduced with permission.[75] Copyright 2023 Springer Nature.

higher stability than the reference devices with PTAA-based WBG cells and MPA2FPh-BT-BA-free NBG cells.

2.3 SAM-HTMs based on other anchoring groups

Other types of anchoring groups are also used in the design of SAM-HTMs. 2-Cyanoacrylic acid (CA) is a traditional anchoring group widely used in organic dyes for DSSCs, giving a hint for the molecular design of SAMs for PSCs. The CA groups can function as efficient passivation sites for the perovskite films owing to their Lewis-base characteristic to form a coordination interaction with Pb^{2+} to reduce the harmful trap states at the interface.[76] The high polarity of the CA group has potential in enabling good solubility of the corresponding compounds in polar solvents (*e.g.*, ethyl acetate, ethanol). Guo *et al.* incorporated CA as an anchoring group into D–A-type HTMs to afford MPA-BT-CA (3-(7-(4-(bis(4-methoxyphenyl)amino)phenyl)benzo[*c*][1,2,5]thiadiazol-4-yl)-2-cyanoacrylic acid) (Fig. 12a).[77] The D–A-type framework may help to increase the hole extraction and reduce the exciton recombination rate in PSCs.[78,79] The introduction of
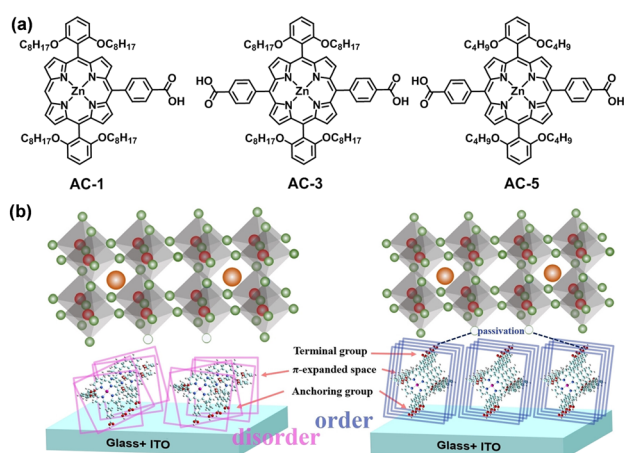

Fig. 10 (a) Chemical structures of AC-1, AC-3, and AC-5. (b) Schematic diagram of interfacial changes between ITO/SAM/perovskite. Reproduced with permission.[74] Copyright 2023 Wiley-VCH GmbH.
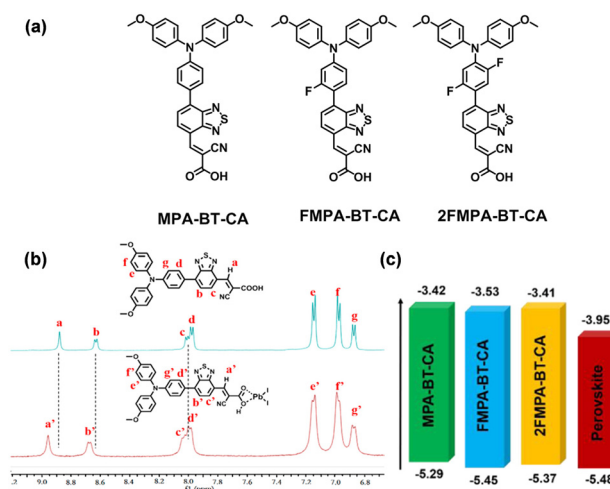
Fig. 12 (a) Molecular structures of MPA-BT-CA, FMPA-BT-CA, and 2FMPA-BT-CA. (b) Comparison of the ^{1}H NMR spectra of MPA-BT-CA with or without PbI$_2$. Reproduced with permission.[77] Copyright 2023 American Chemical Society. (c) Diagram of the device energy level alignment. Reproduced with permission.[80] Copyright 2023 American Chemical Society.

1448 | *Mol. Syst. Des. Eng.*, 2023, **8**, 1440–1455

This journal is © The Royal Society of Chemistry and IChemE 2023

the CA group enhances the interaction between the carboxyl groups and the Pb^{2+} ions (Fig. 12b). MPA-BT-CA also shows several prominent properties such as good alcohol solubility, energy level modulation, and interfacial modification, leading to an impressive champion PCE of 21.2% with good long-term and thermal stabilities. The unencapsulated devices showed extraordinary stability with PCE above 20% after storage in N_2 atmosphere for 8 months. The encapsulated devices retained more than 98% of their initial PCE after two weeks while that of the reference MPA-BT (without an anchoring group) devices dropped to 70% under ambient atmosphere (72% RH).

Later in 2022, they further utilized a fluorination strategy to improve the buried interfacial interaction between the HTL and perovskite, attaining FMPA-BT-CA (3-(7-(4-(bis(4-methoxyphenyl)amino)-2-fluorophenyl)benzo[*c*]-[1,2,5]thiadiazol-4-yl)-2-cyanoacrylic acid) and 2FMPA-BT-CA (3-(7-(4-(bis(4-methoxyphenyl)amino)-2,5-difluorophenyl)benzo-[*c*][1,2,5]thiadiazol-4-yl)-2-cyanoacrylic acid) (Fig. 12a).[80] The incorporation of fluorine resulted in deeper HOMO energy levels, larger dipole moments and favourable molecular packing in the film due to the noncovalent interactions between the fluorine and hydrogen atom or electron-rich groups (Fig. 12c). A PCE of 22.37% was achieved for FMPA-BT-CA-based PSCs. Due to improved film morphology and passivation modified by fluorinated FMPA-BT-CA, PSCs retained more than 90% of the initial PCE after 1000 h of illumination in a N_2 glove box, while the MPA-BT-CA-based devices decayed more than 20% of the initial PCE.

Considering that the conjugated molecular structure can stabilize the electron-rich arylamines, Zhu *et al.* incorporated conjugated linkers instead of alkyl linkers to connect the anchoring group (CA) with electron-rich arylamine units (carbazole and triphenylamine) to create a series of SAMs (Fig. 13a).[81] The effect of conjugation length on the self-assembly behavior of SAM was studied. The conjugated linkers not only enhance the charge-transporting of SAMs, but also stabilize the electron-rich arylamines through electron/charge delocalization. Most of the triple-cation PSCs based on conjugation SAMs can afford over 20% PCE. Among them, MPA-Ph-CA-based PSCs achieved a PCE of 22.53% (certified 22.12%) with excellent stability (>95% of the initial PCE) under one-sun constant irradiation for 800 h (Fig. 13b and c).

Despite the impressive progress in the development of SAMs for Pb-based PSCs, there is significant interest in designing new SAMs for less toxic tin PSCs. Diau and co-workers developed a series of X-shaped quinoxaline-based D–A SAM HTMs (PQx, PQxD, TQx, and TQxD), using cyano and/or carboxylic units as anchoring groups and quinoxaline as an electron-withdrawing group, for tin PSCs (Fig. 14).[82] The thiophene/phenyl units have no significant effect on the energy levels. With two anchoring groups present at both ends of the quinoxaline core, these X-shaped SAMs have relatively stronger anchoring capacity to the ITO surface to
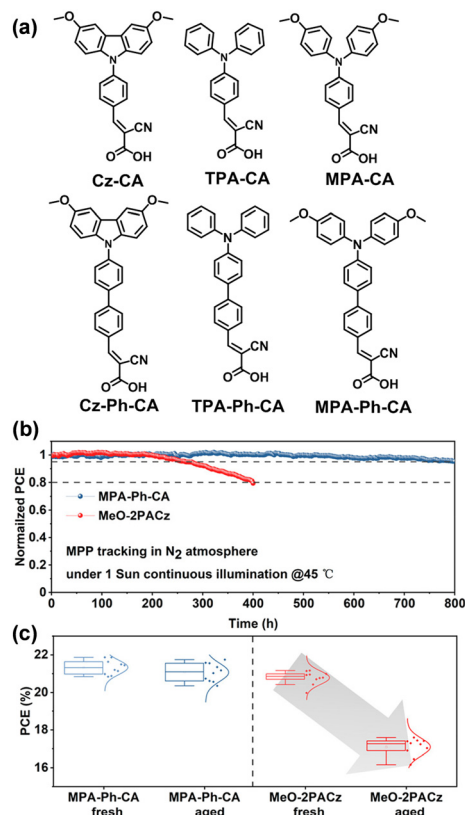

Fig. 13 (a) Molecular structures of Cz-CA, TPA-CA, MPA-CA, Cz-Ph-CA, TPA-Ph-CA, and MPA-Ph-CA. (b) MPP tracking of PSCs under 1 sun continuous illumination. (c) Statistical distribution of PCE values of PSCs based on fresh and aged SAMs. Reproduced with permission.[81] Copyright 2022 American Chemical Society.

form better molecular arrangement.[83] The thiophene units in TQx and TQxD were conducive to forming smooth and uniform tin perovskite nanocrystals with excellent morphology, crystallinity, and film roughness. Tin PSCs based on TQxD and TQx exhibited a PCE of 8.3% and 8.0%, respectively, which was higher than those of corresponding devices with PQxD (7.1%) and PQx (6.1%).

Due to the sensitivity of the ITO substrate to an acidic environment, the strong acidic anchors are detrimental to the long-term stability of the devices.[84–86] The acidity-
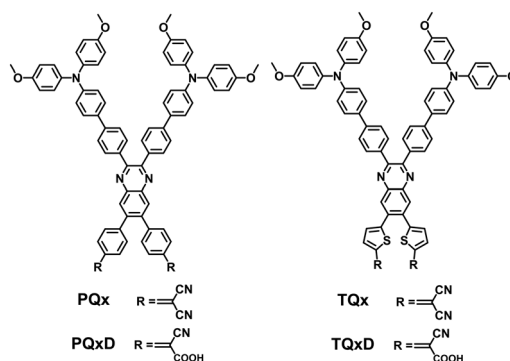

Fig. 14 Molecular structures of PQx, PQxD, TQx, and TQxD.

This journal is © The Royal Society of Chemistry and IChemE 2023

Mol. Syst. Des. Eng., 2023, **8**, 1440–1455 | **1449**

weakened boric acid anchor significantly reduces ITO corrosion and improves device stability. Wu *et al.* reported a boric acid-anchoring HTM MTPA-BA ((4-(di-*p*-tolylamino) phenyl)boronic acid) (Fig. 15a).[87] The HTM with boric acid can easily chemisorb on the ITO surface by formation of stable B–O–In linkage, exhibiting high environmental stability (Fig. 15b and c). Moreover, the boric acid-anchoring HTLs exhibit excellent hole selectivity and efficient defect passivation, which improves the FF performance. MTPA-BA-based PSCs realized a PCE of 22.6% with a prominent FF of 85.2%. MA/Br-free and wide-bandgap PSCs using boric acid-anchoring SAMs also show enhanced FF performance. More importantly, the MTPA-BA-based devices showed high long-term stability, with $T_{90} > 2400$ h, which is five times that of 2PACz-based PSCs.

In order to increase the wettability of the surface of SAM-HTLs, Wu *et al.* combined the cyanovinyl phosphonic acid (CPA) anchoring group with hydrophobic methoxyl-substituted triphenylamine (MPA) to develop an amphiphilic

SAM-HTM MPA-CPA ((2-(4-(bis(4-methoxyphenyl)amino) phenyl)-1-cyanovinyl)phosphonic acid) (Fig. 15d).[88] The CPA anchoring group not only forms a superwetting bilayer HTL between perovskite and the ITO substrate, but also minimizes the buried interfacial defects through Pb–N and Pb–O bonds (Fig. 15e and f). Compared with PTAA and 2PACz, the perovskite film deposited on MPA-CPA exhibits higher photoluminescence quantum yield and longer Shockley–Read–Hall lifetime (Fig. 15g and h), which represents the reduction of the nonradiative recombination at the buried interface. The MPA-CPA-based p–i–n PSC exhibits a remarkable certified PCE of 25.4% with an enhanced prominent V_{oc} of 1.21 V and a high FF of 84.7%. Meanwhile, the 1 cm² devices and 10 cm² minimodules achieved a PCE of 23.4% and 22.0%, respectively. The encapsulated modules exhibited an excellent stability with 90% of the initial PCE after 2000 h of illumination at around 45 °C in ambient air (30–40% RH) due to the minimized buried interfacial defects.
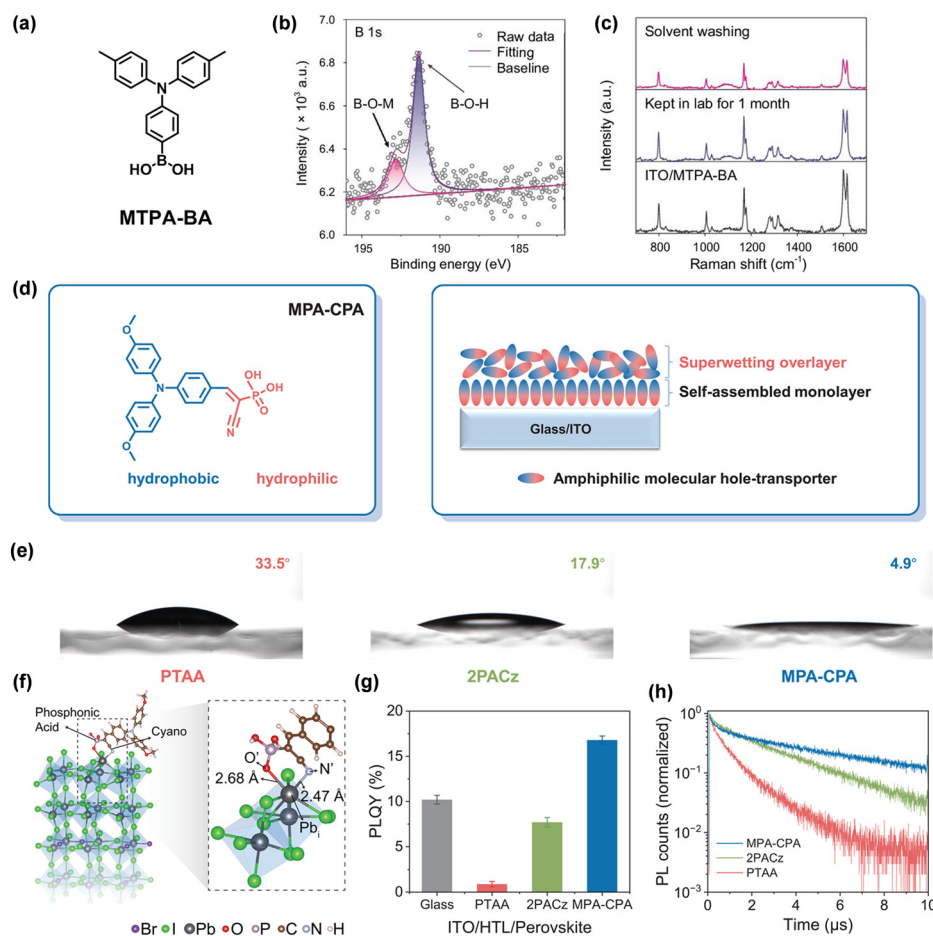
Fig. 15 (a) Molecular structures of MTPA-BA. (b) B 1s XPS result of the ITO/MTPA–BA sample. (c) Raman spectra of ITO/MTPA–BA under different treatments. Reproduced with permission.[87] Copyright 2023 Oxford University Press on behalf of China Science Publishing & Media Ltd. (d) Molecular structure of MPA-CPA (left) and schematic depiction of the bilayer stack of MPA-CPA molecules on an ITO-glass substrate (right). (e) Contact angles of the perovskite precursor solution on different SAMs. (f) Optimized structure of the passivated surface. Photoluminescence quantum yield (g) and photoluminescence decays (h) of perovskite films on different substrates. Reproduced with permission.[88] Copyright 2023, The American Association for the Advancement of Science.

Table 1 The photoelectric properties and device structure of PSCs based on different SAM-HTMs

SAM	Device structure	Area (cm²)	V_{oc} (V)	J_{sc} (mA cm⁻²)	FF (%)	PCE (%)	Ref.
V1036	ITO/V1036/C4/$Cs_{0.05}(MA_{0.17}FA_{0.83})_{0.95}Pb(I_{0.83}Br_{0.17})_3$/$C_{60}$/BCP/Cu	0.16	1.09	21.4	76.5	17.8	55
MeO-2PACz	ITO/MeO-2PACz/$MA_{0.05}FA_{0.95}Pb(I_{0.95}Br_{0.05})_3$/$C_{60}$/BCP/Cu	0.16	1.12	23.5	80.6	21.2	56
2PACz	ITO/2PACz/$Cs_{0.05}(MA_{0.17}FA_{0.83})_{0.95}Pb(I_{0.83}Br_{0.17})_3$/$C_{60}$/BCP/Cu	0.108	1.158	21.7	80.91	20.28[a]	56
Me-4PACz	Ag/AZO/a-Si(p)/a-Si(i)/c-Si(n)/a-Si(i)/nc-SiOx(n)/ITO/Me-4PACz/$Cs_{0.05}(FA_{0.77}MA_{0.23})_{0.95}Pb(I_{0.77}Br_{0.23})_3$/$C_{60}$/$SnO_2$/IZO/Ag/LiF	1.0599	1.900	19.23	79.40	29.15[a]	58
Br-2PACz	ITO/Be-2PACz/$Cs_{0.25}FA_{0.75}Sn_{0.5}Pb_{0.5}I_3$/$C_{60}$/BCP/Ag	0.04	0.81	32.14	74.94	19.51	59
DC-PA	ITO/DC-PA/IAHA/$Cs_{0.05}MA_{0.15}FA_{0.80}PbI_3$/$C_{60}$/BCP/Ag	0.105	1.16	24.66	82.45	23.59	60
CbzNaph	ITO/CbzNaph/$Cs_{0.05}MA_{0.15}FA_{0.80}PbI_3$/$C_{60}$/BCP/Ag	0.105	1.17	24.69	83.39	24.1	61
4PACz	ITO/4PACz/$Cs_{0.05}MA_{0.15}FA_{0.80}PbI_3$/$C_{60}$/BCP/Ag	0.105	1.07	23.20	58.43	14.5	61
CbzPh	ITO/CbzPh/$Cs_{0.05}MA_{0.15}FA_{0.80}PbI_3$/$C_{60}$/BCP/Ag	0.105	1.13	23.43	73.06	19.2	61
4PADCB	ITO/4PADCB/$FA_{0.8}Cs_{0.2}Pb(I_{0.6}Br_{0.4})_3$/$C_{60}$/$SnO_2$/Cu	0.05	1.30	17.84	78.70	18.28	62
4PADCB	ITO/4PADCB/$FA_{0.8}Cs_{0.2}Pb(I_{0.6}Br_{0.4})_3$/$C_{60}$/$SnO_2$/IZO/PEDOT:PSS/$FA_{0.6}MA_{0.3}Cs_{0.1}Sn_{0.5}Pb_{0.5}I_3$/$C_{60}$/$SnO_2$/Cu	1.044	2.12	15.19	82.6	26.6[a]	62
BCB-C4PA	ITO/BCB-C4PA/$Cs_{0.07}FA_{0.9}MA_{0.03}Pb(I_{0.92}Br_{0.08})_3$/$C_{60}$/BCP/Ag	—	1.13	24.4	80	22.2	63
TPT-P6	ITO/SAM/$Cs_{0.05}MA_{0.12}FA_{0.83}Pb(I_{0.85}Br_{0.15})_3$/$C_{60}$/BCP/Ag	0.09	1.125	23.49	81.08	21.43	64
TPT-S6	ITO/SAM/$Cs_{0.05}MA_{0.12}FA_{0.83}Pb(I_{0.85}Br_{0.15})_3$/$C_{60}$/BCP/Ag	0.09	0.998	21.50	75.31	16.16	64
TPT-C6	ITO/SAM/$Cs_{0.05}MA_{0.12}FA_{0.83}Pb(I_{0.85}Br_{0.15})_3$/$C_{60}$/BCP/Ag	0.09	1.077	23.32	75.46	18.87	64
Br-2EPT	FTO/Br-2EPT/$Cs_{0.05}(FA_{0.92}MA_{0.08})_{0.95}Pb(I_{0.92}Br_{0.08})_3$/$C_{60}$/BCP/Cu	0.11406	1.098	24.51	81.05	21.81[a]	65
Br-2EPO	FTO/Br-2EPO/$Cs_{0.05}(FA_{0.92}MA_{0.08})_{0.95}Pb(I_{0.92}Br_{0.08})_3$/$C_{60}$/BCP/Cu	0.094237	1.074	24.25	80.74	21.02	66
Br-2EPSe	FTO/Br-2EPSe/$Cs_{0.05}(FA_{0.92}MA_{0.08})_{0.95}Pb(I_{0.92}Br_{0.08})_3$/$C_{60}$/BCP/Cu	0.094237	1.12	23.95	83.56	22.26[a]	66
DMACPA	ITO/$Cs_{0.05}(FA_{0.95}MA_{0.05})_{0.95}Pb(I_{0.95}Br_{0.05})_3$ (DMACPA)/PEABr/$PC_{61}BM$/BCP/Ag	0.0802	1.189	25.66	83.24	25.39[a]	67
3PATAT-C3	ITO/3PATAT-C3/$Cs_{0.05}MA_{0.15}FA_{0.80}PbI_{2.75}Br_{0.25}$/$EDAI_2$/$C_{60}$/BCP/Ag	0.1	1.13	24.5	83.0	23.0	70
TPA-PT-C6	ITO/TPA-PT-C6/CA-Br /$MAPbI_3$/$PC_{61}BM$/BCP/Ag	1.02	1.039	21.80	77.35	17.49	71
Spiro-Acid	ITO/$Cs_{0.05}(FA_{0.85}MA_{0.15})_{0.95}Pb(I_{0.85}Br_{0.15})_3$/$C_{60}$/BCP/Ag	0.09	0.99	22.20	82.6	18.15	72
MC-43	ITO/MC-43/$MAPbI_3$/$PC_{61}BM$/Ag	0.09	1.08	20.1	80.0	17.3	46
TPA	ITO/TPA/$MAPbI_3$/$PC_{61}BM$/Ag	0.09	1.06	19.4	76.9	15.9	46
EADR03	ITO/EADR03/$Cs_{0.05}MA_{0.12}FA_{0.83}Pb(I_{0.85}Br_{0.15})_3$/LiF/$C_{60}$/BCP/Cu	—	1.156	22.9	80	21.2	73
EADR04	ITO/EADR04/$Cs_{0.05}MA_{0.12}FA_{0.83}Pb(I_{0.85}Br_{0.15})_3$/LiF/$C_{60}$/BCP/Cu	—	1.164	22.6	80	21.0	73
AC-1	ITO/AC-1/CsFAMAPb/$PC_{61}BM$/BCP/Ag	0.1	1.084	18.83	80.49	16.43	74
AC-3	ITO/AC-3/ CsFAMAPb/$PC_{61}BM$/BCP/Ag	0.1	1.108	24.27	82.56	22.20	74
AC-5	ITO/AC-5/CsFAMAPb/$PC_{61}BM$/BCP/Ag	0.1	1.130	24.42	84.05	23.19	74
MPA2FPh-BT-BA	ITO/MPA2FPh-BT-BA/$FA_{0.8}Cs_{0.2}Pb(I_{0.6}Br_{0.4})_3$/$C_{60}$/ALD-$SnO_2$/Cu	0.0576	1.289	17.96	82.46	19.09[a]	75
MPA2FPh-BT-BA	ITO/MPA2FPh-BT-BA/$FA_{0.8}Cs_{0.2}Pb(I_{0.6}Br_{0.4})_3$/$C_{60}$/ALD-$SnO_2$/IZO/PEDOT: PSS/MPA2FPh-BT-BA/$FA_{0.6}MA_{0.3}Cs_{0.1}Pb_{0.5}Sn_{0.5}I_3$/$C_{60}$/ALD-$SnO_2$/Cu	0.0574	2.105	15.22	82.3	26.3[a]	75
MPA-BT-CA	ITO/MPA-BT-CA/$(FA_{0.17}MA_{0.94}PbI_{3.01})_{0.95}(PbCl_2)_{0.05}$/$C_{60}$/BCP/Ag	0.037	1.13	22.25	84.8	21.24	77
FMPA-BT-CA	ITO/FMPA-BT-CA/$FA_{0.15}MA_{0.85}PbI_{2.8}Cl_{0.2}$/$C_{60}$/BCP/Cu	0.037	1.151	23.33	83.6	22.37	80
2FMPA-BT-CA	ITO/2FMPA-BT-CA/$FA_{0.15}MA_{0.85}PbI_{2.8}Cl_{0.2}$/$C_{60}$/BCP/Cu	0.037	1.143	22.81	83.1	21.68	80
MPA-Ph-CA	ITO/MPA-Ph-CA/$Cs_{0.05}(FA_{0.92}MA_{0.08})_{0.95}Pb(I_{0.92}Br_{0.08})_3$/$PC_{61}BM$/$C_{60}$/BCP/Ag	0.0663	1.136	23.23	84.00	22.12[a]	81
PQxD	ITO/PQxD/$FASnI_3$/C_{60}/BCP/Ag	0.0225	0.455	19.97	66.6	6.1	82
PQx	ITO/PQx/$FASnI_3$/C_{60}/BCP/Ag	0.0225	0.542	19.28	68.1	7.1	82
TQxD	ITO/TQxD/$FASnI_3$/C_{60}/BCP/Ag	0.0225	0.574	21.05	68.8	8.3	82
TQx	ITO/TQx/$FASnI_3$/C_{60}/BCP/Ag	0.0225	0.546	21.30	69.0	8.0	82
MTPA-BA	ITO/MTPA-BA/$Cs_{0.05}(FA_{0.95}MA_{0.05})_{0.95}Pb(I_{0.95}Br_{0.05})_3$/$PC_{61}BM$/$C_{60}$/BCP/Ag	0.0625	1.14	23.24	85.2	22.62	87
MPA-CPA	ITO/MPA-CPA/$Cs_{0.05}(FA_{0.95}MA_{0.05})_{0.95}Pb(I_{0.95}Br_{0.05})_3$/$C_{60}$/BCP/Ag	0.0805	1.210	24.77	84.65	25.39[a]	88

[a] Certified PCE. All the other PCEs were measured in-house at the respective laboratories.

3 Conclusions

Inverted PSCs have rapidly developed to achieve a champion PCE of around 26%, since the importance and potential of inverted PSCs for commercialization of single-junction and tandem solar cells are recognized. The encouraging development in organic HTMs especially SAMs recently plays a critical role in the improvement of both PCE and stability of inverted PSCs. In this review, we summarize the recent important progress in SAM-based HTMs from 2018 by different anchoring groups and molecular skeletons, mainly focusing on the design of molecules and the performance in devices (as summarized in Table 1).

Although the first PSC based on SAM was fabricated late in 2018, SAM-HTMs have been considered to be an excellent alternative of polymer HTMs like PTAA due to a great many advantages, such as low cost, tunable bandgap, good interface stability, easy fabrication, excellent scalability and compatibility for either tandem solar cells or large-area devices. On the basis of the discussion in this review, some conclusions can be drawn for the future design of SAM-HTMs. For the anchoring groups of SAMs, phosphonic acid and cyanoacetic acid are more attractive, because of their fast adsorption dynamics and strong bonding strength. Regarding the functional group, carbazole, triphenylamine and phenothiazine derivatives are good candidates because of their strong electron-donating ability and conjugated structures. In addition, halogens can be introduced into the functional groups to regulate the work function and passivate the perovskite defects. Although the most efficient SAMs currently choose non-conjugated alkyl linkers to obtain an ordered molecular arrangement, more conjugated linkers can be examined to improve the hole-transport ability of SAMs.

However, there are still some challenges and issues that need to be addressed. Herein, we propose the following research directions worthy of attention for future studies. (1) Up to now, most of the highly efficient inverted PSCs are realized by SAMs based on phosphonic acid as an anchoring group. Nevertheless, the corrosion of the ITO surface by acidic species remains a problem to influence the long-term stability of PSCs. New kinds of anchoring groups still need to be explored for the design of SAMs. (2) As is known to all, the efficient passivation and suitable wettability can help to fabricate perovskite with better quality and stability, whereas the exact effect of precise functional groups in SAMs on the perovskite deposition and crystallization process is not clear. In this sense, more studies are required to investigate the relationship between the functional groups and perovskite film quality. (3) For future commercialization, developing SAMs compatible with the fabrication of large-area devices is important. In this regard, some efficient SAM-HTLs are processed by spin-coating, which is not a good choice for the manufacture of large-area devices.[89,90] Whether the SAM-HTL can exhibit similar high performance to advanced large-area film processing methods such as blade coating, vacuum deposition and roll-to-roll printing remains a question, since the crystallization process is quite different when changing the film processing methods. For further application in large-area PSC modules, SAMs should have suitable wettability on the perovskite film. (4) Till now, most of the anchoring groups in the reported SAM-HTMs are used to connect to the transparent conductive oxide side, and no functional group is available to directly bind to perovskite. New design of double-anchored SAM-HTMs is of interest to be investigated whether it can provide a better interfacial contact or promote the crystallization of perovskite, also considering the balance with other properties such as wettability for the improvement of device efficiency and stability.

Except for performance and stability, green chemistry and upscaling have been attracting the interest of the photovoltaic community for the near future commercialization of the PSCs. Polymer HTMs like PTAA usually need to be dissolved in toluene or chlorobenzene. These two solvents are both toxic and environmentally harmful, increasing the difficulty for future commercialization. Compared with polymer HTMs, SAMs exhibit excellent solubility in green solvents such as ethanol and isopropanol due to the hydrophilic anchoring groups. The SAM-HTL can be easily fabricated by dip-coating, spin-coating or chemical bath deposition with green-solvent solutions. At the same time, SAMs are viewed to be easier to scale since they are characterized by a low cost, simple synthetic route and do not suffer from batch to batch variability. Currently, most PSCs are fabricated by spin-coating. Although spin-coating can afford high-quality films, it is disadvantageous in that only small amounts of the material are deposited onto substrates, resulting in more than 90% of material wastage. This may limit the application of spin-coating in large-scale productions. Therefore, the chemical bath deposition method of SAMs is more appealing to large-area PSCs and modules, as well as perovskite-based tandem solar cells. In conclusion, we believe that the development of SAM-HTMs will be conducive to further improving the performance of inverted PSCs.

Author contributions

Conflicts of interest

There are no conflicts to declare.

Acknowledgements

1452 | *Mol. Syst. Des. Eng.*, 2023, **8**, 1440–1455

This journal is © The Royal Society of Chemistry and IChemE 2023

Notes and references

1 L. Hammarström and S. Hammes-Schiffer, *Acc. Chem. Res.*, 2009, **42**, 1859–1860.

2 M. A. Green, A. Ho-Baillie and H. J. Snaith, *Nat. Photonics*, 2014, **8**, 506–514.

3 A. K. Jena, A. Kulkarni and T. Miyasaka, *Chem. Rev.*, 2019, **119**, 3036–3103.

4 A. Yella, H.-W. Lee, H. N. Tsao, C. Yi, A. K. Chandiran, M. K. Nazeeruddin, E. W.-G. Diau, C.-Y. Yeh, S. M. Zakeeruddin and M. Grätzel, *Science*, 2011, **334**, 629–634.

5 X. Luo, X. Lin, F. Gao, Y. Zhao, X. Li, L. Zhan, Z. Qiu, J. Wang, C. Chen, L. Meng, X. Gao, Y. Zhang, Z. Huang, R. Fan, H. Liu, Y. Chen, X. Ren, J. Tang, C.-H. Chen, D. Yang, Y. Tu, X. Liu, D. Liu, Q. Zhao, J. You, J. Fang, Y. Wu, H. Han, X. Zhang, D. Zhao, F. Huang, H. Zhou, Y. Yuan, Q. Chen, Z. Wang, S. Liu, R. Zhu, J. Nakazaki, Y. Li and L. Han, *Sci. China: Chem.*, 2022, **65**, 2369–2416.

6 A. Kojima, K. Teshima, Y. Shirai and T. Miyasaka, *J. Am. Chem. Soc.*, 2009, **131**, 6050–6051.

7 National Renewable Energy Laboratory, *Best research-cell efficiencies chart*, https://www.nrel.gov/pv/assets/pdfs/best-research-cell-efficiencies.pdf (accessed July, 2023).

8 J.-Y. Shao and Y.-W. Zhong, *Bull. Chem. Soc. Jpn.*, 2021, **94**, 632–640.

9 H. Li, Z. Liu, Z. Chen, S. Tan, W. Zhao, Y. Li, J. Shi, H. Wu, Y. Luo, D. Li and Q. Meng, *Sci. China: Chem.*, 2022, **65**, 1185–1195.

10 S. Yang, W. Fu, Z. Zhang, H. Chen and C.-Z. Li, *J. Mater. Chem. A*, 2017, **5**, 11462–11482.

11 H. D. Pham, T. C.-J. Yang, S. M. Jain, G. J. Wilson and P. Sonar, *Adv. Energy Mater.*, 2020, **10**, 1903326.

12 Y. Li, Q. Zhang, L. Liu, D. Wang, Z. Liu, N. Yuan, J. Ding, Q. Wang and S. Liu, *Sci. China: Chem.*, 2023, **66**, 185–194.

13 X. Sun, Z. Zhu and Z. a. Li, *Front. Optoelectron.*, 2022, **15**, 46.

14 D. Luo, W. Yang, Z. Wang, A. Sadhanala, Q. Hu, R. Su, R. Shivanna, G. F. Trindade, J. F. Watts, Z. Xu, T. Liu, K. Chen, F. Ye, P. Wu, L. Zhao, J. Wu, Y. Tu, Y. Zhang, X. Yang, W. Zhang, R. H. Friend, Q. Gong, H. J. Snaith and R. Zhu, *Science*, 2018, **360**, 1442–1446.

15 X. Zheng, Y. Hou, C. Bao, J. Yin, F. Yuan, Z. Huang, K. Song, J. Liu, J. Troughton, N. Gasparini, C. Zhou, Y. Lin, D.-J. Xue, B. Chen, A. K. Johnston, N. Wei, M. N. Hedhili, M. Wei, A. Y. Alsalloum, P. Maity, B. Turedi, C. Yang, D. Baran, T. D. Anthopoulos, Y. Han, Z.-H. Lu, O. F. Mohammed, F. Gao, E. H. Sargent and O. M. Bakr, *Nat. Energy*, 2020, **5**, 131–140.

16 Y. Hou, E. Aydin, M. De Bastiani, C. Xiao, F. H. Isikgor, D.-J. Xue, B. Chen, H. Chen, B. Bahrami, A. H. Chowdhury, A. Johnston, S.-W. Baek, Z. Huang, M. Wei, Y. Dong, J. Troughton, R. Jalmood, A. J. Mirabelli, T. G. Allen, E. Van Kerschaver, M. I. Saidaminov, D. Baran, Q. Qiao, K. Zhu, S. De Wolf and E. H. Sargent, *Science*, 2020, **367**, 1135–1140.

17 Z. Yu, Z. Yang, Z. Ni, Y. Shao, B. Chen, Y. Lin, H. Wei, Z. J. Yu, Z. Holman and J. Huang, *Nat. Energy*, 2020, **5**, 657–665.

18 F. Li, X. Deng, F. Qi, Z. Li, D. Liu, D. Shen, M. Qin, S. Wu, F. Lin, S.-H. Jang, J. Zhang, X. Lu, D. Lei, C.-S. Lee, Z. Zhu and A. K. Y. Jen, *J. Am. Chem. Soc.*, 2020, **142**, 20134–20142.

19 R. Azmi, E. Ugur, A. Seitkhan, F. Aljamaan, A. S. Subbiah, J. Liu, G. T. Harrison, M. I. Nugraha, M. K. Eswaran, M. Babics, Y. Chen, F. Xu, T. G. Allen, A. u. Rehman, C.-L. Wang, T. D. Anthopoulos, U. Schwingenschlögl, M. De Bastiani, E. Aydin and S. De Wolf, *Science*, 2022, **376**, 73–77.

20 Z. Li, B. Li, X. Wu, S. A. Sheppard, S. Zhang, D. Gao, N. J. Long and Z. Zhu, *Science*, 2022, **376**, 416–420.

21 X. Sun, Z. Zhu and Z. Li, *Front. Optoelectron.*, 2022, **15**, 46.

22 Q. Jiang, J. Tong, Y. Xian, R. A. Kerner, S. P. Dunfield, C. Xiao, R. A. Scheidt, D. Kuciauskas, X. Wang, M. P. Hautzinger, R. Tirawat, M. C. Beard, D. P. Fenning, J. J. Berry, B. W. Larson, Y. Yan and K. Zhu, *Nature*, 2022, **611**, 278–283.

23 Q. Tan, Z. Li, G. Luo, X. Zhang, B. Che, G. Chen, H. Gao, D. He, G. Ma, J. Wang, J. Xiu, H. Yi, T. Chen and Z. He, *Nature*, 2023, **620**, 545–551.

24 J.-Y. Shao, D. Li, J. Shi, C. Ma, Y. Wang, X. Liu, X. Jiang, M. Hao, L. Zhang, C. Liu, Y. Jiang, Z. Wang, Y.-W. Zhong, S. F. Liu, Y. Mai, Y. Liu, Y. Zhao, Z. Ning, L. Wang, B. Xu, L. Meng, Z. Bian, Z. Ge, X. Zhan, J. You, Y. Li and Q. Meng, *Sci. China: Chem.*, 2022, **66**, 10–64.

25 J. Urieta-Mora, I. García-Benito, A. Molina-Ontoria and N. Martín, *Chem. Soc. Rev.*, 2018, **47**, 8541–8571.

26 X. Sun, D. Zhao and Z. a. Li, *Chin. Chem. Lett.*, 2018, **29**, 219–231.

27 J.-Y. Shao and Y.-W. Zhong, *Chin. J. Org. Chem.*, 2021, **41**, 1447–1465.

28 G. Tang, P. You, Q. Tai, A. Yang, J. Cao, F. Zheng, Z. Zhou, J. Zhao, P. K. L. Chan and F. Yan, *Adv. Mater.*, 2019, **31**, 1807689.

29 C. Bi, Q. Wang, Y. Shao, Y. Yuan, Z. Xiao and J. Huang, *Nat. Commun.*, 2015, **6**, 7747.

30 Y. Li, J.-F. Liao, H. Pan and G. Xing, *Sol. RRL*, 2022, **6**, 2200647.

31 F. Bella, G. Griffini, J.-P. Correa-Baena, G. Saracco, M. Grätzel, A. Hagfeldt, S. Turri and C. Gerbaldi, *Science*, 2016, **354**, 203–206.

32 J.-Y. Jeng, K.-C. Chen, T.-Y. Chiang, P.-Y. Lin, T.-D. Tsai, Y.-C. Chang, T.-F. Guo, P. Chen, T.-C. Wen and Y.-J. Hsu, *Adv. Mater.*, 2014, **26**, 4107–4113.

33 S. Sajid, A. M. Elseman, H. Huang, J. Ji, S. Dou, H. Jiang, X. Liu, D. Wei, P. Cui and M. Li, *Nano Energy*, 2018, **51**, 408–424.

34 N. Arora, M. I. Dar, A. Hinderhofer, N. Pellet, F. Schreiber, S. M. Zakeeruddin and M. Grätzel, *Science*, 2017, **358**, 768–771.

35 J. Cao, B. Wu, J. Peng, X. Feng, C. Li and Y. Tang, *Sci. China: Chem.*, 2019, **62**, 363–369.

36 T. Wang, D. Ding, H. Zheng, X. Wang, J. Wang, H. Liu and W. Shen, *Sol. RRL*, 2019, **3**, 1900045.

37 W. Han, G. Ren, Z. Li, M. Dong, C. Liu and W. Guo, *J. Energy Chem.*, 2020, **46**, 202–207.

38 L. Bertoluzzi, C. C. Boyd, N. Rolston, J. Xu, R. Prasanna, B. C. O'Regan and M. D. McGehee, *Joule*, 2020, **4**, 109–127.

This journal is © The Royal Society of Chemistry and IChemE 2023

Mol. Syst. Des. Eng., 2023, **8**, 1440–1455 | **1453**

39 S. Chen, X. Dai, S. Xu, H. Jiao, L. Zhao and J. Huang, *Science*, 2021, **373**, 902–907.

40 X. Sun, Z. Li, X. Yu, X. Wu, C. Zhong, D. Liu, D. Lei, A. K.-Y. Jen, Z. Li and Z. Zhu, *Angew. Chem.*, 2021, **60**, 7227–7233.

41 H. Xu, Z. Liang, J. Ye, Y. Zhang, Z. Wang, H. Zhang, C. Wan, G. Xu, J. Zeng, B. Xu, Z. Xiao, T. Kirchartz and X. Pan, *Energy Environ. Sci.*, 2023, DOI: **10.1039/D3EE02591H**.

42 E. D. Jung, A. K. Harit, D. H. Kim, C. H. Jang, J. H. Park, S. Cho, M. H. Song and H. Y. Woo, *Adv. Mater.*, 2020, **32**, 2002333.

43 A. Al-Ashouri, E. Köhnen, B. Li, A. Magomedov, H. Hempel, P. Caprioglio, J. A. Márquez, A. B. Morales Vilches, E. Kasparavicius, J. A. Smith, N. Phung, D. Menzel, M. Grischek, L. Kegelmann, D. Skroblin, C. Gollwitzer, T. Malinauskas, M. Jošt, G. Matič, B. Rech, R. Schlatmann, M. Topič, L. Korte, A. Abate, B. Stannowski, D. Neher, M. Stolterfoht, T. Unold, V. Getautis and S. Albrecht, *Science*, 2020, **370**, 1300–1309.

44 J. Liu, M. De Bastiani, E. Aydin, G. T. Harrison, Y. Gao, R. R. Pradhan, M. K. Eswaran, M. Mandal, W. Yan, A. Seitkhan, M. Babics, A. S. Subbiah, E. Ugur, F. Xu, L. Xu, M. Wang, A. u. Rehman, A. Razzaq, J. Kang, R. Azmi, A. A. Said, F. H. Isikgor, T. G. Allen, D. Andrienko, U. Schwingenschlögl, F. Laquai and S. De Wolf, *Science*, 2022, **377**, 302–306.

45 F. Ali, C. Roldán-Carmona, M. Sohail and M. K. Nazeeruddin, *Adv. Energy Mater.*, 2020, **10**, 2002989.

46 E. Yalcin, M. Can, C. Rodriguez-Seco, E. Aktas, R. Pudi, W. Cambarau, S. Demic and E. Palomares, *Energy Environ. Sci.*, 2019, **12**, 230–237.

47 L. Zhang and J. M. Cole, *ACS Appl. Mater. Interfaces*, 2015, **7**, 3427–3455.

48 S. P. Pujari, L. Scheres, A. T. M. Marcelis and H. Zuilhof, *Angew. Chem., Int. Ed.*, 2014, **53**, 6322–6356.

49 R. Qiao and L. Zuo, *J. Mater. Res.*, 2018, **33**, 387–400.

50 S. Y. Kim, S. J. Cho, S. E. Byeon, X. He and H. J. Yoon, *Adv. Energy Mater.*, 2020, **10**, 2002606.

51 L. Zuo, Q. Chen, N. De Marco, Y.-T. Hsieh, H. Chen, P. Sun, S.-Y. Chang, H. Zhao, S. Dong and Y. Yang, *Nano Lett.*, 2017, **17**, 269–275.

52 P. B. Paramonov, S. A. Paniagua, P. J. Hotchkiss, S. C. Jones, N. R. Armstrong, S. R. Marder and J.-L. Brédas, *Chem. Mater.*, 2008, **20**, 5131–5133.

53 S. A. Paniagua, A. J. Giordano, O. L. Smith, S. Barlow, H. Li, N. R. Armstrong, J. E. Pemberton, J.-L. Brédas, D. Ginger and S. R. Marder, *Chem. Rev.*, 2016, **116**, 7117–7158.

54 L. Zhang and J. M. Cole, *ACS Appl. Mater. Interfaces*, 2015, **7**, 3427–3455.

55 A. Magomedov, A. Al-Ashouri, E. Kasparavičius, S. Strazdaite, G. Niaura, M. Jošt, T. Malinauskas, S. Albrecht and V. Getautis, *Adv. Energy Mater.*, 2018, **8**, 1801892.

56 A. Al-Ashouri, A. Magomedov, M. Roß, M. Jošt, M. Talaikis, G. Chistiakova, T. Bertram, J. A. Márquez, E. Köhnen, E. Kasparavičius, S. Levcenco, L. Gil-Escrig, C. J. Hages, R. Schlatmann, B. Rech, T. Malinauskas, T. Unold, C. A. Kaufmann, L. Korte, G. Niaura, V. Getautis and S. Albrecht, *Energy Environ. Sci.*, 2019, **12**, 3356–3369.

57 M. Jošt, T. Bertram, D. Koushik, J. A. Marquez, M. A. Verheijen, M. D. Heinemann, E. Köhnen, A. Al-Ashouri, S. Braunger, F. Lang, B. Rech, T. Unold, M. Creatore, I. Lauermann, C. A. Kaufmann, R. Schlatmann and S. Albrecht, *ACS Energy Lett.*, 2019, **4**, 583–590.

58 A. Al-Ashouri, E. Köhnen, B. Li, A. Magomedov, H. Hempel, P. Caprioglio, J. A. Márquez, A. B. M. Vilches, E. Kasparavicius, J. A. Smith, N. Phung, D. Menzel, M. Grischek, L. Kegelmann, D. Skroblin, C. Gollwitzer, T. Malinauskas, M. Jošt, G. Matic, B. Rech, R. Schlatmann, M. Topic, L. Korte, A. Abate, B. Stannowski, D. Neher, M. Stolterfoht, T. Unold, V. Getautis and S. Albrecht, *Science*, 2020, **370**, 1300–1309.

59 M. Pitaro, J. S. Alonso, L. Di Mario, D. Garcia Romero, K. Tran, T. Zaharia, M. B. Johansson, E. M. J. Johansson and M. A. Loi, *J. Mater. Chem. A*, 2023, **11**, 11755–11766.

60 X. Deng, F. Qi, F. Li, S. Wu, F. R. Lin, Z. Zhang, Z. Guan, Z. Yang, C.-S. Lee and A. K.-Y. Jen, *Angew. Chem., Int. Ed.*, 2022, **61**, e202203088.

61 W. Jiang, F. Li, M. Li, F. Qi, F. R. Lin and A. K.-Y. Jen, *Angew. Chem., Int. Ed.*, 2022, **61**, e202213560.

62 R. He, W. Wang, Z. Yi, F. Lang, C. Chen, J. Luo, J. Zhu, J. Thiesbrummel, S. Shah, K. Wei, Y. Luo, C. Wang, H. Lai, H. Huang, J. Zhou, B. Zou, X. Yin, S. Ren, X. Hao, L. Wu, J. Zhang, J. Zhang, M. Stolterfoht, F. Fu, W. Tang and D. Zhao, *Nature*, 2023, **618**, 80–86.

63 W. Wang, K. Wei, L. Yang, J. Deng, J. Zhang and W. Tang, *Mater. Horiz.*, 2023, **10**, 2609–2617.

64 E. Li, C. Liu, H. Lin, X. Xu, S. Liu, S. Zhang, M. Yu, X.-M. Cao, Y. Wu and W.-H. Zhu, *Adv. Funct. Mater.*, 2021, **31**, 2103847.

65 A. Ullah, K. H. Park, H. D. Nguyen, Y. Siddique, S. F. A. Shah, H. Tran, S. Park, S. I. Lee, K.-K. Lee, C.-H. Han, K. Kim, S. Ahn, I. Jeong, Y. S. Park and S. Hong, *Adv. Energy Mater.*, 2022, **12**, 2103175.

66 A. Ullah, K. H. Park, Y. Lee, S. Park, A. B. Faheem, H. D. Nguyen, Y. Siddique, K.-K. Lee, Y. Jo, C.-H. Han, S. Ahn, I. Jeong, S. Cho, B. Kim, Y. S. Park and S. Hong, *Adv. Funct. Mater.*, 2022, **32**, 2208793.

67 Q. Tan, Z. Li, G. Luo, X. Zhang, B. Che, G. Chen, H. Gao, D. He, G. Ma, J. Wang, J. Xiu, H. Yi, T. Chen and Z. He, *Nature*, 2023, **620**, 545–551.

68 D. Moia, A. Szumska, V. Vaissier, M. Planells, N. Robertson, B. C. O'Regan, J. Nelson and P. R. F. Barnes, *J. Am. Chem. Soc.*, 2016, **138**, 13197–13206.

69 D. Moia, V. Vaissier, I. López-Duarte, T. Torres, M. K. Nazeeruddin, B. C. O'Regan, J. Nelson and P. R. F. Barnes, *Chem. Sci.*, 2014, **5**, 281–290.

70 M. A. Truong, T. Funasaki, L. Ueberricke, W. Nojo, R. Murdey, T. Yamada, S. Hu, A. Akatsuka, N. Sekiguchi, S. Hira, L. Xie, T. Nakamura, N. Shioya, D. Kan, Y. Tsuji, S. Iikubo, H. Yoshida, Y. Shimakawa, T. Hasegawa, Y. Kanemitsu, T. Suzuki and A. Wakamiya, *J. Am. Chem. Soc.*, 2023, **145**, 7528–7539.

71 E. Li, E. Bi, Y. Wu, W. Zhang, L. Li, H. Chen, L. Han, H. Tian and W.-H. Zhu, *Adv. Funct. Mater.*, 2020, **30**, 1909509.

1454 | *Mol. Syst. Des. Eng.*, 2023, **8**, 1440–1455

This journal is © The Royal Society of Chemistry and IChemE 2023

72 W. Li, M. Cariello, M. Méndez, G. Cooke and E. Palomares, *ACS Appl. Energy Mater.*, 2023, **6**, 1239–1247.

73 E. Aktas, N. Phung, H. Köbler, D. A. González, M. Méndez, I. Kafedjiska, S.-H. Turren-Cruz, R. Wenisch, I. Lauermann, A. Abate and E. Palomares, *Energy Environ. Sci.*, 2021, **14**, 3976–3985.

74 C.-M. Hung, C.-L. Mai, C.-C. Wu, B.-H. Chen, C.-H. Lu, C.-C. Chu, M.-C. Wang, S.-D. Yang, H.-C. Chen, C.-Y. Yeh and P.-T. Chou, *Angew. Chem., Int. Ed.*, 2023, **62**, e202309831.

75 J. Zhu, Y. Luo, R. He, C. Chen, Y. Wang, J. Luo, Z. Yi, J. Thiesbrummel, C. Wang, F. Lang, H. Lai, Y. Xu, J. Wang, Z. Zhang, W. Liang, G. Cui, S. Ren, X. Hao, H. Huang, Y. Wang, F. Yao, Q. Lin, L. Wu, J. Zhang, M. Stolterfoht, F. Fu and D. Zhao, *Nat. Energy*, 2023, **8**, 714–724.

76 T. Wu, Y. Wang, Z. Dai, D. Cui, T. Wang, X. Meng, E. Bi, X. Yang and L. Han, *Adv. Mater.*, 2019, **31**, 1900605.

77 Y. Wang, Q. Liao, J. Chen, W. Huang, X. Zhuang, Y. Tang, B. Li, X. Yao, X. Feng, X. Zhang, M. Su, Z. He, T. J. Marks, A. Facchetti and X. Guo, *J. Am. Chem. Soc.*, 2020, **142**, 16632–16643.

78 Y. Wang, W. Chen, L. Wang, B. Tu, T. Chen, B. Liu, K. Yang, C. W. Koh, X. Zhang, H. Sun, G. Chen, X. Feng, H. Y. Woo, A. B. Djurišić, Z. He and X. Guo, *Adv. Mater.*, 2019, **31**, 1902781.

79 S. A. Ok, B. Jo, S. Somasundaram, H. J. Woo, D. W. Lee, Z. Li, B.-G. Kim, J. H. Kim, Y. J. Song, T. K. Ahn, S. Park and H. J. Park, *Nat. Commun.*, 2018, **9**, 4537.

80 Q. Liao, Y. Wang, M. Hao, B. Li, K. Yang, X. Ji, Z. Wang, K. Wang, W. Chi, X. Guo and W. Huang, *ACS Appl. Mater. Interfaces*, 2022, **14**, 43547–43557.

81 S. Zhang, R. Wu, C. Mu, Y. Wang, L. Han, Y. Wu and W.-H. Zhu, *ACS Mater. Lett.*, 2022, **4**, 1976–1983.

82 S. N. Afraj, C.-H. Kuan, J.-S. Lin, J.-S. Ni, A. Velusamy, M.-C. Chen and E. W.-G. Diau, *Adv. Funct. Mater.*, 2023, **33**, 2213939.

83 C.-Y. Lo, D. Kumar, S.-H. Chou, C.-H. Chen, C.-H. Tsai, S.-H. Liu, P.-T. Chou and K.-T. Wong, *ACS Appl. Mater. Interfaces*, 2016, **8**, 27832–27842.

84 M. A. Reijme, M. P. de Jong, D. P. L. Simons, M. Schok, L. J. van Ijzendoorn, A. W. Denier van der Gon, H. H. Brongersma and M. J. A. de Voigt, *Nucl. Instrum. Methods Phys. Res., Sect. B*, 2002, **194**, 346–354.

85 T. S. Bejitual, K. Ramji, A. J. Kessman, K. A. Sierros and D. R. Cairns, *Mater. Chem. Phys.*, 2012, **132**, 395–401.

86 M. P. de Jong, L. J. van Ijzendoorn and M. J. A. de Voigt, *Appl. Phys. Lett.*, 2000, **77**, 2255–2257.

87 H. Guo, C. Liu, H. Hu, S. Zhang, X. Ji, X.-M. Cao, Z. Ning, W.-H. Zhu, H. Tian and Y. Wu, *Natl. Sci. Rev.*, 2023, **10**, nwad057.

88 S. Zhang, F. Ye, X. Wang, R. Chen, H. Zhang, L. Zhan, X. Jiang, Y. Li, X. Ji, S. Liu, M. Yu, F. Yu, Y. Zhang, R. Wu, Z. Liu, Z. Ning, D. Neher, L. Han, Y. Lin, H. Tian, W. Chen, M. Stolterfoht, L. Zhang, W.-H. Zhu and Y. Wu, *Science*, 2023, **380**, 404–409.

89 N.-G. Park and K. Zhu, *Nat. Rev. Mater.*, 2020, **5**, 333–350.

90 S.-W. Lee, S. Bae, D. Kim and H.-S. Lee, *Adv. Mater.*, 2020, **32**, 2002202.

This journal is © The Royal Society of Chemistry and IChemE 2023

Mol. Syst. Des. Eng., 2023, **8**, 1440–1455 | 1455